Aqueous carbonation of cement bypass dust for reuse in cement: Potassium chloride removal, hydration reactivity and mechanical properties

Construction and Building Materials 506 (2026) 145004

Contents lists available at ScienceDirect

Construction and Building Materials

journal homepage: www.elsevier.com/locate/conbuildmat

Aqueous carbonation of cement bypass dust for reuse in cement: Potassium chloride removal, hydration reactivity and mechanical properties

Francesca Bonfante [a], Pedro Humbert [b], Davide Garufi [b], Jean-Marc Tulliani [a], Paola Palmero [a], Giuseppe Ferrara [a,*]

[a] Politecnico di Torino, INSTM R.U. PoliTO-LINCE, Department of Applied Science and Technology, Corso Duca Degli Abruzzi 24, Torino (TO) 10129, Italy
[b] CRH Innovation EMAT, De Klencke 10-12, Amsterdam 1083 HL, the Netherlands

ARTICLE INFO

Keywords:
Carbon capture and utilisation
Cement bypass dust
Wet carbonation
Supplementary cementitious materials
Carbon footprint

ABSTRACT

At present, Cement Bypass Dust (CBPD) is landfilled even if characterised by elevated levels of free lime because of high chlorides and sulphates contents. Thus, this study investigated the possibility of reusing CBPD in cement mortars after an aqueous carbonation treatment. Emphasis was given on the optimisation of KCl removal during the carbonation process. To this end, a range of liquid-to-solid ratios and washing-carbonating cycles were investigated. Subsequently, isothermal calorimetry and compressive strength tests on mortars, were done on the as received and carbonated CBPD. Finally, a comparative analysis of CO_2 emissions, substitution percentage and strength class, based on the data from different types of standard cement, was conducted to frame CBPD-based cements within the current commercial classifications. The samples with reduced chlorides content, showed similar reactivity when analysed with calorimetry. However, CBPD first hydrated then, carbonated (CBPDhc), stood out as the material with higher heat rate and the better mechanical performances with a relative strength of −26.9 % respect to the reference sample.

1. Introduction

Cement is the most widely used building material, with a world production that reached 4.1 billion tons in 2022 [1]. With the increasing global demand for housing and infrastructure, cement production is projected to continue its steady growth in the coming years [2]. In this context, growing attention has been focusing on the significant global emissions associated to cement production and the need of their reduction. The recently published CEMBUREAU 2050 Net Zero Roadmap [2], identifies five key strategies for achieving net-zero emissions. Two of these approaches have been identified as having the most significant impact: *i*) the introduction of carbon capture and storage technologies (CCUS) within clinker production and *ii*) the substitution of clinker with alternative materials in cement production. Of these, clinker substitution with so-called supplementary cementitious materials (SCMs) is regarded as the most straightforward approach for reducing the carbon footprint of Ordinary Portland Cement (OPC). Nevertheless, the availability of the most common SCMs, such as ground-granulated blast-furnace slag and fly ashes, is expected to decline, especially in Europe, since the plants from which they come from are shifting their production processes [1]. A material that has been the focus of extensive research for its potential reuse in cement and concrete is cement bypass dust (CBPD) [3–9]. This alkaline, waste material is formed during clinker manufacturing, accounting for approximately 2–5 % by mass of clinker produced [10]. Unlike the previously mentioned waste, CBPD production is expected to continuously increase in the coming years as a direct consequence of rising cement and clinker production.

CBPD is retrieved from the kiln tail chamber via a bypass that has been installed for the extraction of volatile and harmful elements (e.g. chlorine, sulphur, alkali, etc.) from the flue gases that are derived from the increasing adoption of alternative fuels [11]. Due to its collection from a subsequent stage, at temperatures approximating 1000°C, CBPD is characterised by elevated levels of free lime, chlorides and sulphates. Furthermore, CBPD composition demonstrates significant variability both within a single plant and across different plants. Due to its unstable and variable chemical composition, the recycling of CBPD for cement production is only feasible for a maximum of 5 % of the total [12], with

* Corresponding author.
E-mail addresses: francesca.bonfante@polito.it (F. Bonfante), phumbert@crh.com, paola.palmero@polito.it (P. Humbert), dgarufi@crh.com (D. Garufi), jeanmarc.tulliani@polito.it (J.-M. Tulliani), giuseppe.ferrara@polito.it (G. Ferrara).

https://doi.org/10.1016/j.conbuildmat.2025.145004
Received 6 August 2025; Received in revised form 26 November 2025; Accepted 22 December 2025
Available online 23 December 2025

the remaining part being disposed of via landfill. However, given the potential for CBPD to generate issues such as groundwater contamination if not properly disposed, and considering its status as a valuable chlorine-alkali-rich material, it is essential to promote its reuse, specifically to partially replace cement. Currently, CBPD reuse has also been studied in other fields, including use as a soil stabiliser [13], a filler in asphalt concrete [14], an industrial salt source [15,16] and as a feedstock for carbon capture [17–19]. Due to its chemical composition and alkaline nature, CBPD emerged as a suitable feedstock for carbon capture technologies. In fact, as previously demonstrated in a study by the authors [18], the CBPD exhibited a high affinity for carbonation, with significant uptake of CO_2 achieved through optimised conditions of reaction time and temperature. This resulted in a CO_2 content of 23.2 % by mass in the carbonated CBPD. Furthermore, the carbonation by an aqueous route facilitates the concurrent reduction in chlorides content, as previously reported in several research studies [16,20,21], which is of paramount importance in the case of applications in reinforced concrete structures.

In this study, the two above-mentioned CEMBUREAU approaches for the decarbonation of cement production, namely i) the implementation of CCUS technologies and ii) the partial replacement of clinker with SCMs, are merged, in an innovative vision of the carbonation process as an upcycling pretreatment for CBPD. Indeed, this study investigates the possibility of reusing CBPD as cement replacement after an aqueous carbonation treatment. The potential reuse of the treated powder as SCM is intended to meet both the strength requirements and the chemical composition requirements, particularly with regard to the chlorides content.

Thus, the present study aims to further optimise the carbonation process with a focus on chloride removal. The objective is to define a mineralisation process that induces direct storage of CO_2, while efficiently removing chlorides, producing a suitable feedstock to be used in cement blends. To this end, a range of liquid-to-solid ratios and washing-carbonating cycles are investigated. After this, isothermal calorimetry and compressive strength tests on mortars were executed on the as-received and carbonated CBPD. These tests were adopted to investigate the hydration heat of the carbonated material and to determine whether reuse as SCM could be a viable option for the carbonated CBPD. This research examines the possible impacts of calcium carbonate and potassium chloride concentrations in CBPD on the mechanical characteristics of mortars with CBPD partial replacement. To elucidate the impact of the study, the findings are compared with conventional cement types, specifically CEM I, CEM II and CEM III, and cement incorporating the carbonated CBPD to evaluate their carbon footprint. The comparative analysis encompasses not only the attained strength class but also the relative CO_2 emissions.

2. Materials and methods

2.1. Materials characterisation

The CBPD was supplied by CRH Innovation Center for Sustainable Construction (Amsterdam, The Netherlands). The material was collected from an Irish plant, directly in the form of a powder. Laser diffraction was used to determine the particle size distributions of the CBPD and ordinary Portland cement used in this study. Measurements were made under dry conditions using a Malvern Mastersizer 3000 AERO S laser granulometer (Malvern Pan'alytical, Worcestershire, UK).

The chemical composition of CBPD and ordinary Portland cement (CEM I 52.5 N VVM Cement, Cementbouw) was determined using a Rigaku Supermini 2000 X-ray fluorescence spectrometer (Rigaku, Tokyo, Japan) and is given in Table 1. As shown in the table, CaO, K_2O, Cl and SiO_2 are the dominant components of CBPD, accounting for 39.1, 16.9, 14.8 and 5.9 %, respectively. CBPD has a lower content of CaO and SiO_2 compared to cement, due to the high amount of chlorides.

*LOI – Loss on ignition, calculated as the weight loss reached at 1000°C

The crystalline phases were detected by X-ray diffraction (Malvern Pan'alytical Empyrean, Worcestershire, UK) in the Bragg-Brentano configuration and with a PIXcel detector. Measurements were taken over a range of 2θ from 5 to 70° at 40 kV and 40 mA with a step size of 0.06° and 23 s per step. The results are shown in Fig. 1. Main minerals found in CBPD (Fig. 1.a) were lime (CaO, JCPDF card number 96–900–8606), sylvite and halite/sylvite (KCl and K(Na)Cl, JCPDF card numbers 96–900–3113 and 96–900–3180), Portlandite ($Ca(OH)_2$,

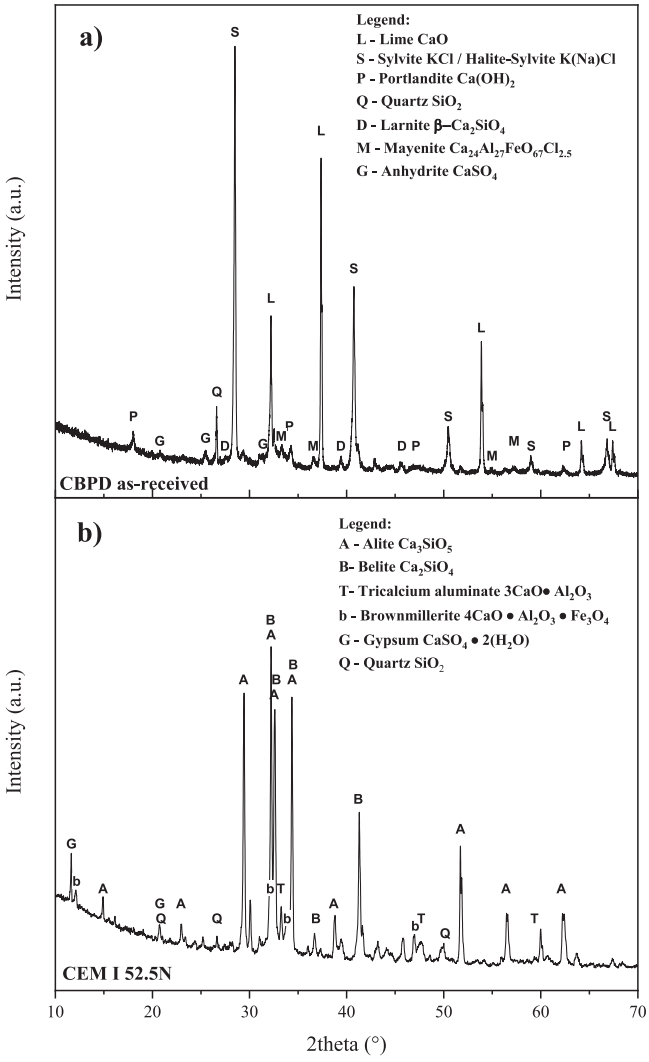

Fig. 1. XRD patterns of a) CBPD and b) ordinary Portland cement (CEM I 52.5 N).

Table 1
Chemical composition of CBPD and Ordinary Portland cement.

Chemical composition (wt%)	CaO	K_2O	Cl	SiO_2	Fe_2O_3	Al_2O_3	MgO	Na_2O	SO_3	LOI
CBPD	39.1	16.9	14.8	5.9	1.5	2.1	1.1	1.8	2.6	13.4
CEM I 52.5 N	62.2	1.2	0.1	18.9	2.3	4.3	1.6	0.2	3.8	4.7

JCPDF card number 96–100–1788), larnite (Ca_2SiO_4, JCPDF card number 96–901–2791), quartz (SiO_2, JCPDF card number 96–900–9667), anhydrite ($CaSO_4$, JCPDF card number 96–500–0041) and mayenite ($Ca_{24}Al_{27}FeO_{67}Cl_{2.5}$, JCPDF card number 96–901–5595). Fig. 1. b shows the XRD pattern of ordinary Portland cement in which the common cement phases were identified. In particular, tricalcium silicate (Alite, C_3S, JCPDF card number 00–049–0442), dicalcium silicate (Belite, β-C_2S, JCPDF card number 00–033–0302), brownmillerite or tricalcium aluminate (C_3A, JCPDF card number 00–038–1429), tetracalcium aluminoferrite (C_4AF, JCPDF card number 00–030–0226), quartz (SiO_2, JCPDF card number 96–900–9667) and calcium sulphate (gypsum, $CaSO_4{\cdot}2H_2O$, JCPDF card number 00–021–0816) were detected.

X-ray diffraction measurements were also taken over a range of 2θ from 27.5 to 32.5° at 40 kV and 40 mA with a step size of 0.002° and 1 s per step. This measure was adopted to study in detail the presence of KCl in the powder before and after the treatments. This analysis was conducted by performing a calibration based on the area under the main KCl peak and the respective content of KCl, obtained by the total removal, collection and weight of the salt.

Thermogravimetric/Differential Thermal Analysis (TG-DTA, LABSYS EVO from Setaram, Caluire, France) was used to qualitatively and quantitatively assess changes in material composition. The analyses were carried out at temperatures up to 1050°C at a rate of 10 °C/min in alumina crucibles. Nitrogen was used as a carrier gas at a flow rate of 20 mL/min. The morphology of the particles was characterised by Field-Emission Scanning Electron Microscopy (FESEM, Hitachi S4000, Tokyo, Japan). Prior to FESEM characterisation, the as-received, hydrated and carbonated CBPD samples were coated with a layer of gold (approximately 30 nm) using SPI module sputtering.

2.2. Experimental design

2.2.1. Accelerated aqueous carbonation

Direct aqueous carbonation was carried out using the system previously described by Bonfante et al. [9]. The set-up consists of a 500 mL flask immersed in a crystalliser on a heating plate to ensure temperature homogenisation. The flask is kept under continuous stirring during carbonation to ensure that the slurry remains mixed. A pipe connects the CO_2 bottle (5.0 grade, SIAD, Italy) to the flask, which is partially closed by a drilled cap to maintain ambient pressure. Direct aqueous carbonation is carried out with a liquid-to-solid ratio (L/S) of 3 and a flow rate of CO_2 (99.9 vol%) set at 150 L/h based on a previous study from the authors [18]. In the same study, the CO_2 uptake was optimised by reaction time and temperature and the optimised parameters, 60 min and 40°C respectively, are kept constant in this study. After the carbonation process, the slurry is subjected to a centrifugation step and the resulting residue is dried in an oven at 60°C for 24 h, leading to the carbonated CPBPD (CBPDc). The dried powder is adopted for chemical characterisation, isothermal calorimetry tests and mechanical characterisation.

TG-DTA was used for the quantification of carbon dioxide (CO_2) [22]. In fact, in previous study from the authors, this technique was proved to provide reliable estimate of the CO_2 content in carbonated samples. The CO_2 content is determined as the difference between the mass of the sample measured at 550°C ($m_{550°C}$) and 850°C ($m_{850°C}$), divided by the mass of the sample before the thermal treatment (initial mass, m_i, Eq. 1). Indeed, the weight loss occurring between 550°C and 850°C is commonly associated with the complete decomposition of calcium carbonate [23–25].

$$m_{CO_2}(\%) = \frac{(m_{550°C} - m_{850°C})}{m_i}\ 100 \tag{1}$$

To quantify the CO_2 captured by a material, it is common to refer to the CO_2 uptake, defined as the mass of CO_2 captured (ΔCO_2) by the initial mass of the material used. Eq. 2 was derived in the previous study [18] in order to correctly calculate the CO_2 uptake for the CBPD specifically. In fact, the common equation adopted for the CO_2 uptake assumes that the mass changes before and after the carbonation are fully attributable to the CO_2 captured, i.e. Δm_{hy} and Δm_{KCl}, the mass variations resulting from hydration and salt removal, respectively, are negligible. However, the cement bypass dust undergoes significant mass alterations during the carbonation process, not only due to the formation of calcium carbonate, but also due to the hydration of some phases and KCl dissolution and removal.

$$\%CO_{2\ \text{uptake}} = \frac{\Delta CO_2}{m_i} \cong \frac{\%CO'_{2\ \text{content}} \times \left(1 + \frac{\Delta m_{hy} + \Delta m_{KCl}}{m_i}\right) - \%CO_{2\ \text{initial}}}{1 - \left(\%CO'_{2\ \text{content}}\right)} \tag{2}$$

In order to study the effects of aqueous carbonation on the material, CBPD dust was subjected to testing in three distinct phases: as-received (CBPDar), after hydration (CBPDhy), and after carbonation (CBPDc). CBPDhy was prepared by dispersing the dust in distilled water, with L/S ratio of 3, for one hour. Then a centrifuge/drying process was used. This setup, using hydration pretreatment without gas injection, was proposed to recreate CBPDc process conditions to study hydration effects alone.

2.2.2. Salt removal

Once demonstrated the correctness of the set-up and related parameters for the aqueous carbonation, the focus of this experimental part was to optimise the process towards the maximum salt removal. The liquid-to-solid ratio was identified as the key parameter related to the salt removal. Therefore, starting from the initial L/S = 3, this ratio was progressively increased, to study the effect of water dilution on the salt removal efficacy. The progression, aimed at obtaining the overall trend with the minimum number of tests, was defined by approximately doubling the parameter at each step until the complete removal of salt was obtained (L/S equal to 3, 5, 10 and 20). Following the hydration stage, the slurry was subjected to centrifugation and drying, as previously outlined. The liquid resulting from the hydration process was collected and dried, with the objective of recovering the salt. This approach enabled the quantification of the salt removed. Once established the effect of the liquid-to-solid ratio on salt removal, three novel configurations for the carbonation process were introduced combining carbonation and washing cycles (see Table 2). This analysis is intended to minimise the L/S ratio while maintaining both carbonation and salt removal efficiency. Specifically, the aqueous carbonation process was repeated with a L/S of 10 (CBPDc10) maintaining unchanged the ratio between the CO_2 flowrate and the sample mass. To achieve complete salt removal, two additional configurations were proposed: CBPDch, involving carbonation of the CBPD with a L/S ratio of 3 and hydration

Table 2
Carbonation process for optimal salt removal (pHi=initial pH value, pHf=final pH value).

Label	Step 1	Step 2
CBPDhy	**Hydration** L/S ratio = 3 t = 60 min, T = 40 °C pHf= 12.6	-
CBPDc	**Carbonation** L/S ratio = 3 t = 60 min, T = 40 °C pHi= 12.6, pHf= 9.0	-
CBPDc10	**Carbonation** L/S ratio = 10 t = 60 min, T = 40 °C pHi= 12.6, pHf= 6.9	-
CBPDch	**Carbonation** L/S ratio = 3 t = 60 min, T = 40 °C pHi= 12.6, pHf= 9.0	**Hydration** L/S ratio = 10 t = 60 min, T_{amb} pH= 11.1
CBPDhc	**Hydration** L/S ratio = 10 t = 60 min, T_{amb} pHf= 12.6	**Carbonation** L/S ratio = 3 t = 60 min, T = 40 °C pHi= 12.7, pHf= 11.6

with an L/S ratio of 10; and CBPDhc, where hydration precedes carbonation.

Following each step, the salt was collected, and its quantity was determined, as previously outlined. In addition, X-ray diffraction and thermogravimetric analyses were conducted on all the powders. The efficiency in terms of carbonation was also investigated.

2.2.3. Isothermal calorimetry

The necessity for reactivity testing of SCMs has increased, particularly for non-conventional SCMs, which are not adequately addressed by conventional tests developed for cement. In this context, the RILEM TC 267-TRM [26] has recently developed novel reactivity tests for SCMs, namely the R^3 reactivity test. This test facilitates the prediction of the mechanical properties of various non-conventional SCMs through isothermal calorimetry and bound water test after seven days [27]. In particular, the calorimetry-based testing method assesses the inherent reactivity of the SCM without the influence of cement hydration [28]. Indeed, the investigation of SCM/cement blends gives rise to a number of challenges, insofar as the hydration of Portland cement and the hydraulic reaction of SCMs occur concurrently, with the potential to affect the reactivity of the components in a mutual way [29]. Consequently, the R^3 method involves the preparation of a paste from portlandite, calcite and a potassium solution (see Table 3), as outlined in the ASTM C1897 [30]. Isothermal calorimetry was also conducted on samples of blended cement and SCMs, to study the hydration of cement pastes partially replaced with CBPD. The cement was replaced with 30 % of CBPD and the paste was prepared with water-to-binder ratio of 0.5 (see Table 3). These parameters were consistent with those set during the preparation of mortars. Heat flow was analysed using an I-Cal 8000 HPC (Calmetrix Inc., Needham, USA) with eight channels. All calorimetries were conducted at a temperature of 40°C, with data collection spanning 168 h. The presented results are the average of two repetitions for each configuration. The cumulative heat release was calculated in accordance with Eq. 3. This equation considers the cumulative heat from 75 min following the mixing, allowing for the stabilisation of the sample temperature, until the conclusion of the measurement.

$$H_{7d} = \frac{H_{75\text{min}-168h}}{m_{SCM}} \tag{3}$$

where: $H_{75\ \text{min}\ -\ 168\ \text{h}}$ denotes the cumulative heat released after the initial 75 min until 168 h, and m_{SCM} refers to the mass of CBPD in the analysed sample. Both R^3 and cement replaced tests were conducted on CBPDar, CBPPDhy and CBPDc to identify the impact of carbonation on the CBPD hydration reactivity and on CBPDc10, CBPDch and CBPDhc to understand how different configurations of the carbonation process could affect the residual reactivity.

* SCM refers to the CBPD powder that is downstream of the specific treatment.

** Potassium solution: for 500 mL of deionized water, 2 g of KOH and 10 g of K_2SO_4.

Table 3
Details of pastes preparation for isothermal calorimetry.

SCM*(g)		Binder (g)		Potassium solution (g)**	$CaCO_3$ (g)
CBPDar	5	$Ca(OH)_2$	15	27	2.5
CBPDhy	5	$Ca(OH)_2$	15	27	2.5
CBPDc	5	$Ca(OH)_2$	15	27	2.5
CBPDc10	5	$Ca(OH)_2$	15	27	2.5
CBPDch	5	$Ca(OH)_2$	15	27	2.5
CBPDhc	5	$Ca(OH)_2$	15	27	2.5
SCM*(g)		**Binder (g)**		**Water (g)**	
REF1	0	CEM I 52.5 N	40	20	
CBPDar	12	CEM I 52.5 N	28	20	
CBPDhy	12	CEM I 52.5 N	28	20	
CBPDc	12	CEM I 52.5 N	28	20	
CBPDc10	12	CEM I 52.5 N	28	20	
CBPDch	12	CEM I 52.5 N	28	20	
CBPDhc	12	CEM I 52.5 N	28	20	

2.2.4. Compressive strength tests

Compressive strength assessments conducted on mortars at 28 days of curing, wherein the binder was replaced up to 30 %, was established as the standard for validating the R^3 test by the aforementioned TC 267-TRM [31]. To this end, the compressive strength of the mortars was measured by means of a hydraulic press machine (FORM+TEST Prüfsysteme MEGA 100–300–30 DM1, Riedlingen, Germany), with a maximum load cell of 300 kN, in force control with a rate of 1.5 kN/s. The reference mortars (40 mm × 40 mm × 160 mm) were prepared using Portland cement (type CEM I 52.5 N), standard CEN sand and demineralised water. The mixing, casting and testing processes were conducted in accordance with the specifications outlined in BS EN 196–1 [32]. The prepared specimens were labelled in accordance with their replacement percentage and the SCM utilised (see Table 4). The compressive strength was determined at a 3, 7 or 28-day curing period at 20°C and 100 % RH conditions. The number of tested samples is reported in Table 4. For each curing time a triplet of prism was cast. Samples were produced in two different experimental campaigns. For each of them a reference series was created.

REF: reference mortars prepared with OPC.

To facilitate the comparison of the results with previous literature, the relative compressive strength ($R_{SCM,relative}$), as determined by Eq. 4, was utilised in accordance with the approach previously proposed by Li et al. [31].

$$R_{SCM.relative} = \frac{R_{SCM} - R_{REF}}{R_{REF}} \times 100 \tag{4}$$

Where: R_{SCM} and R_{REF} are the absolute strength in MPa of the SCM blended cement and the pure OPC, respectively.

2.3. CO_2 emissions reduction

This study sets out to assess the impact of CBPD reuse in cement on its carbon footprint. It is hypothesised that the blend obtained by partial replacement of carbonated CBPD will offer a reduction of CO_2 emissions with respect to the cement adopted. This is due to the combination of clinker substitution and CCU strategies. The reduction resulting from partial clinker substitution can be calculated by applying the percentage of substitution, which indicates the part of cement non-used and, consequently, its foregone production. The current average CO_2 eq emissions for the cement adopted in this study, a European OPC (CEM I 52.5 N), were estimated based on five environmental product declarations (Supplementary Material Table S1), amounting to 791 kg CO_2 eq/ton of cement.

Up to the present day, CBPD is considered to be a waste [33] of cement production, and therefore its initial emissions can be considered equal to zero. Furthermore, the production of CBPD takes place within the cement plant and the material is already in the form of dust and does not require grinding or milling. Thus, transport and pretreatment

Table 4
Details of mortars preparation.

Mix ID	CBPD content (% by mass)	Dimensions and number of samples		
		b x h x l (mm^3)	Number	Curing time (days)
REF	0	40x40x160	18	3, 7, 28
CBPDar-30	30		9	3, 7, 28
CBPDhy-30	30		9	3, 7, 28
CBPDc-30	30		9	3, 7, 28
CBPDc-20	20		3	28
CBPDc-10	10		3	28
CBPDc10–30	30		3	28
CBPDch-30	30		3	28
CBPDhc-30	30		3	28

emissions of CBPD would be minimal. The environmental impact of the carbonation process has not yet been evaluated, since the implementation from laboratory scale to pilot project is still ongoing, but it can be reasonably assumed that its relative emissions would be negligible when compared to that of cement. In light of the previous considerations, the CO_2 emissions of cement blends partially replaced by CBPD were calculated in accordance with Eq. 5. In this equation, R represents the replacement rate, and the CO_2 uptake was recalculated as kg of CO_2 incorporated in the mass of the carbonated dust.

$$CO_{2\ \text{emissions}} \cong avgCO_{2emissions\ CEMI\quad 52.5N}\left[\frac{kgCO_2}{ton\ of\ cement}\right] \times (1-R) - CO_{2\ \text{uptake}}\left[\frac{kgCO_2}{ton\ of\ carb.CBPD}\right] \times R \quad (5)$$

where: $avgCO_{2emissions\ CEM\ I52.5N}$ is the average CO_2 eq emissions for the cement type adopted in this study (CEM I 52.5 N), 791 kg CO_2 eq/ton of cement.

3. Results and discussion

3.1. Effects of CPBD treatments on physical and compositional properties

The particle size distribution of Ordinary Portland cement (CEM I 52.5 N) as well as of the as-received, hydrated and carbonated CBPD is illustrated in Fig. 2. CEM I exhibited a bimodal trend, with a curve mainly located between 1 and 100 μm. CBPDar showed a multimodal frequency curve (Fig. 2.a) exhibiting both ultrafine and coarsened fractions compared to CEM I. CBPDhy displayed a bimodal distribution, with the disappearance of the ultrafine fraction and the increase of the coarser one. Finally, after the carbonation, the dust exhibited a multimodal particle size distribution with the primary frequency peak aligned to that of cement. In conclusion, the cement resulted in the lowest maximum diameter (Fig. 2.b). CBPDar resulted in higher fineness, while both hydration and carbonation caused a shift of the particle size distribution to larger sizes. The changes in the particle size distribution may be related to the variation in the composition of the powder due to the hydration/carbonation treatment. More specifically it is related to the hydration and/or carbonation of lime, and to the removal of part of the salts. The diameter at 10th, 50th and 90th percentile of the cumulative curve distribution (D10, D50 and D90, respectively) of the materials are listed in Table 5. It is noteworthy that, irrespective of the configuration, the particle size distribution of CBPD remains approximately consistent with that of CEM I, indicating no discernible size incompatibility in applications as a cement replacement.

Table 5
Percentile values of the particle size distribution of CEM I, CBPDar, CBPDhy and CBPDc (Relative Standard Deviations in brackets).

Sample	D10 (μm)	D50 (μm)	D90 (μm)
CEM I	3.31 (1.0 %)	12.1 (0.6 %)	31.3 (0.3 %)
CBPDar	0.88 (2.3 %)	8.55 (4.8 %)	69.4 (6.4 %)
CBPDhy	5.22 (1.4 %)	31.8 (1.9 %)	134 (5.8 %)
CBPDc	4.55 (4.9 %)	16.3 (6.2 %)	103 (5.4 %)

As illustrated in Fig. 3.a, the XRD patterns of the as-received, hydrated and carbonated CBPD reveal significant alterations in mineral composition. Prior studies have documented the mineral composition of the as-received material (see Fig. 1), identifying lime and sylvite as the predominant compounds. Following the hydration process, the presence of portlandite becomes evident, indicating the reaction between free lime and water. Additionally, a substantial loss of sylvite was observed and quantified to about 18.5 wt% of the initial mass of the sample in a previous study by the authors [18]. Following hydration, the presence of hydrocalumite ($Ca_4Al_2(OH)_{12}Cl_2{\cdot}4\ H_2O$, JCPDF card number 96–900–9354), a Friedel's salt, was also identified. As discussed in [18], the major compounds participating in the carbonation reactions were the calcium species. Eqs. 6–9 show the reactions between free lime (CaO) and/or portlandite ($Ca(OH)_2$) and CO_2 for the production of calcium carbonate ($CaCO_3$, JCPDF card number 96–702–2028) [34].

$$CO_{2(g)} + H_2O_{(l)} \rightarrow 2H^+_{(aq)} + CO^{2-}_{3(aq)} \quad (6)$$

$$CaO_{(s)} + H_2O_{(l)} \rightarrow Ca(OH)_{2(s)} \quad (7)$$

$$Ca(OH)_{2(s)} \rightarrow Ca^{2+}_{(aq)} + 2OH^-_{(aq)} \quad (8)$$

$$Ca^{2+}_{(aq)} + CO^{2-}_{3(aq)} \rightarrow \quad CaCO_{3(s)} \quad (9)$$

The kinetics of $Ca(OH)_2$ with CO_2 in a humid, low-temperature environment are governed by surface reactions on the $Ca(OH)_2$ particles, in conjunction with the coverage of reaction products on the particle surface. In the preliminary phases of the reaction, the rate of carbonation is subjected to the influence of several factors, including surface area, humidity, temperature, and the concentration of CO_2. As the conversion level rises, the reaction rate is reduced by the extent of the reaction. This is due to the presence of a carbonate coating on the

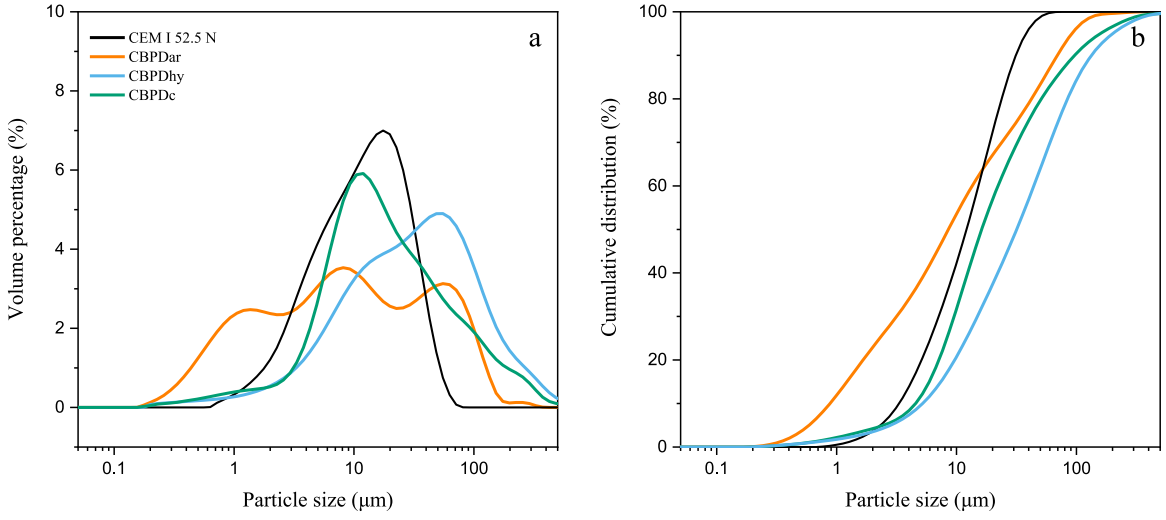

Fig. 2. Particle size distributions of cement (CEM I 52.5 N) and CBPD as-received (CBPDar), hydrated (CBPDhy) and carbonated (CBPDc).

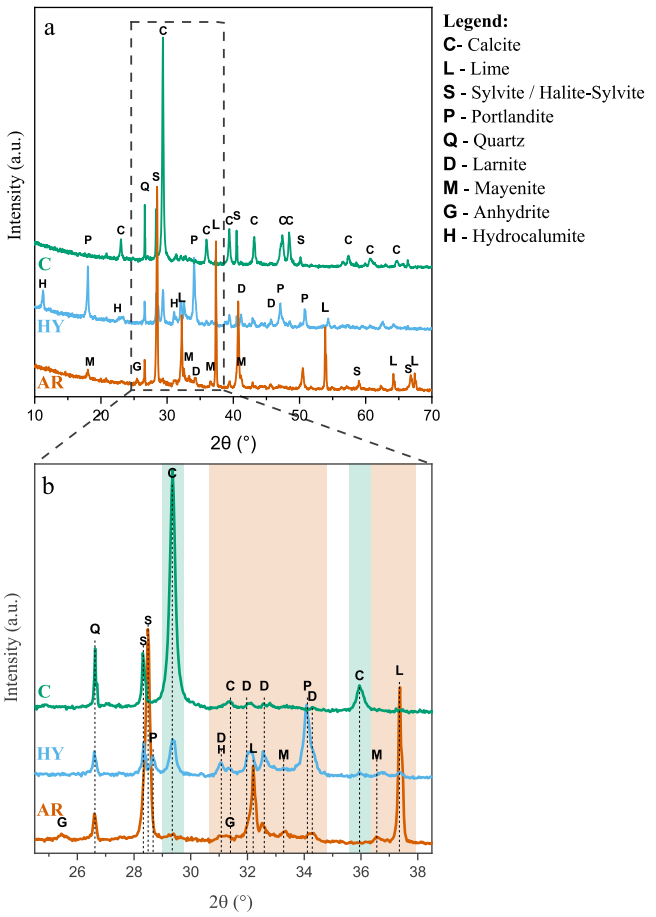

Fig. 3. XRD patterns of cement bypass dust as-received (AR), hydrated (HY) and carbonated (C): **a)** XRD patterns of CBPD; **b)** Comparative intensity of calcite (highlighted in green) and reactive compounds (highlighted in orange).

surfaces of reacting particles [34].

Hydrocalumite was not detected in the carbonated sample due to its pH-dependent stability [35], [36], as the aqueous carbonation reduced the pH of the solution, thereby preventing its formation. In a similar manner to the hydration process, the sylvite phase was reduced by the dissolution of the salt and the centrifugation to separate the solution from the powder. In Fig. 3b, the XRD pattern between 25 and 38 2θ is displayed in greater detail with a view to emphasising the primary peaks of the compound involved in the carbonation process.

Evidently, a small amount of dicalcium silicate persists even after carbonation, suggesting the possibility of further carbonation or the potential for residual hydration reactivity in CBPDc. It is also noteworthy that mayenite was still present after the hydration step but was completely consumed during the carbonation process [37].

Fig. 4 presents the TG-DTA curves of the as-received, hydrated and carbonated CBPD. The initial content of CO_2 obtained from the CBPDar curve was 1.6 %, while hydrated CBPD exhibited an average CO_2 content of 3.82 % (±0.48 %), and carbonated CBPD showed a notable increase to 23.21 % (±0.01 %). Inspection of the DTA curves corroborates the presence of some of the phases that had previously been identified by XRD analysis. The DTA curve of CBPDar confirms the presence of Ca$(OH)_2$, because of the endothermic peak between 400°C and 500°C. A minimum presence of calcium carbonate is associated to the peak at 705°C, and the presence of a potassium-sodium chloride phase (K(Na)Cl) is suggested by the peak at 655°C, which is usually attributed to the melting of this compound [38]. In the hydrated sample, the peaks associated with portlandite and calcium carbonate are also recognisable. A slight shift of these peaks towards higher temperatures is evident

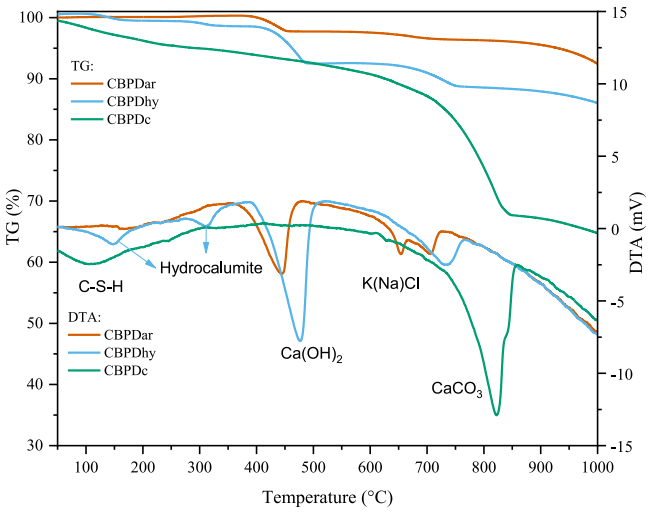

Fig. 4. TGA and DTA curves of CBPD as-received (CBPDar), hydrated (CBPDhy) and carbonated (CBPDc).

when comparing the as-received and hydrated samples; this shift is attributable to the increased content of these compounds, as evidenced by the TG curves [39]. CBPDhy also displays two new DTA peaks at 145°C and 310°C, which can be ascribed to hydrocalumite [40,41], thereby confirming its presence. Finally, the DTA of carbonated CBPD shows a broad endothermic signal at approximately 100 °C associated with the physically absorbed and interlayer water within calcium silicate hydrates (C-S-H) and other hydration phases, and a sharp and substantial endothermic peak between 550° and 850°C, relative to the calcium carbonate decomposition.

Scanning electron microscopy (SEM) observations were conducted on the as-received, hydrated and carbonated samples at varying magnifications (Fig. 5). On the surface of CBPDar it is possible to observe the presence of cubic-shaped grains (Fig. 5a), easily associable to potassium chloride clusters. At higher magnification (Fig. 5d), however, it was possible to observe also hexagonal shaped crystals, typical of portlandite, and the smooth surface typical of free lime. After the hydration a larger amount of portlandite crystal was observed (Figs. 5b and 5e). A significantly differing morphology was observed for carbonated CBPD, wherein the surface of the particles appeared more wrinkled and was covered by ultrafine (100–200 nm) precipitates (Figs. 5c and 5 f), reasonably to be associated with calcium carbonate [42].

3.1.1. *Effect of liquid-to-solid ratio on salt removal*

Fig. 6.a shows the results of the study on the effect of liquid-to-solid ratio (L/S ratio) on the salt removal. The data presented were obtained through the method outlined in Section 2.2.2 (weighing the residue post-drying) and through the estimation of the initial content of KCl in the raw CBPD. As expected, the figure shows that the salt removal efficiency increases with the liquid-to-solid ratio. Despite chlorides content in CBPD is subject to considerable variation, XRD calibration (Supplementary Material Figure S1) permitted the estimation of the content of KCl in CBPDar to 29.24 % with a standard deviation of 1.43 % (Supplementary Material Table S2), calculated as the average of the estimates of the different considered configurations. With the calibration, it was possible to quantify the residual content of KCl in the treated CBPD from the XRD patterns reported in Fig. 6.b. From these results, the L/S ratio of 20 enables the near-total removal of the salt (Fig. 6a), yet it remains detectable through XRD analysis (Fig. 6b).

Given that the adoption of a L/S ratio of 20 for the aqueous carbonation process implies the treatment of a high amount of water, the three configurations previously presented in Table 2 were investigated (the specific mass variations observed are reported in Figure S2 of Supplementary Material). As illustrated in Fig. 7, the primary outcomes

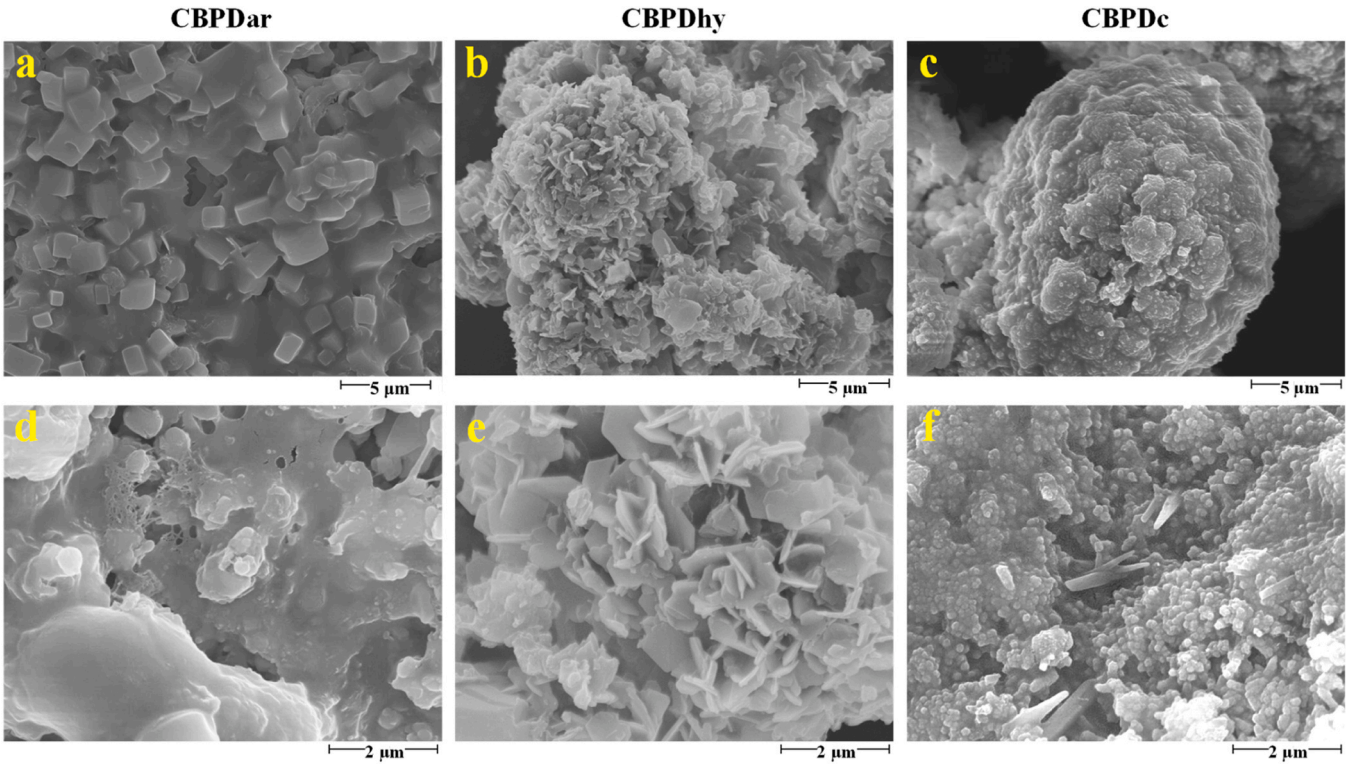

Fig. 5. SEM images of CBPD as-received (a-d), hydrated (b-e) and carbonated (c-f).

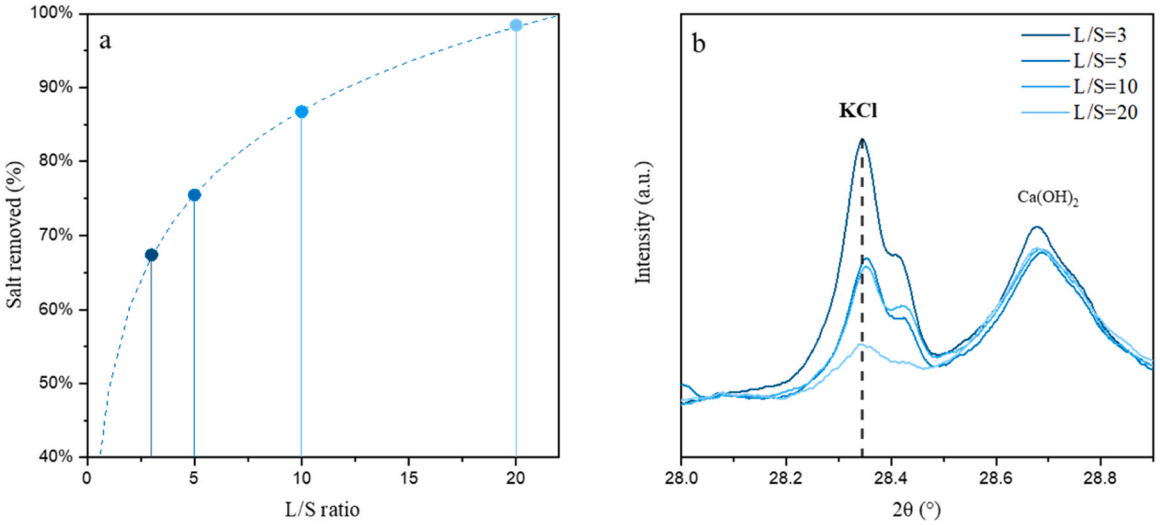

Fig. 6. a) Percentage of salt removed based on the liquid-to-solid ratio, b) XRD patterns of the CBPD hydrated at the different liquid-to-solid ratios.

of the characterisations are displayed, including the TG-DTA (Figs. 7a and 7c) and the XRD analysis (Figs. 7b and 7d). From the TG it was possible to calculate the CO_2 content and CO_2 uptake for each configuration. KCl contents were derived from the calibration model (R^2 0.9999, Fig. S1 of Supplementary Material) based on the XRD analysis (Table 6). The single-step carbonation process with a L/S ratio of 10 (CBPDc10) resulted in the highest final content of CO_2 compared to sample CBPDc carbonated with L/S of 3. This phenomenon can be explained by the fact that CBPDc10 had a comparatively reduced salt content relative to CBPDc, signifying that the percentage calculation was derived from a smaller mass. The validity of this hypothesis can be confirmed through a comparison of the CO_2 uptake results, which demonstrate a greater similarity between the two samples. A comparison of the final pH values obtained from the two experiments revealed a significant difference, with the pH of the slurry from CBPDc equal to 9.0, while the one from CBPDc10 dropped down to 6.9 due to the higher dilution [43]. The carbonation reaction involves the complete consumption of calcium ions more diluted in the solution, resulting in the formation of $CaCO_3$. The excess of CO_2 leads to a more rapid decrease in pH. However, a lower pH typically facilitates the leaching of the calcium that otherwise would not react with CO_2, particularly the calcium bound in silicates and hydrated silicates. CBPDc10 exhibited a minimal weight reduction within the range of the C-S-H and other hydration phases (see Fig. 7.b). This result could corroborate the hypothesis that the majority of calcium underwent reaction to form calcium carbonate, thereby explaining the slight improvement observed in the

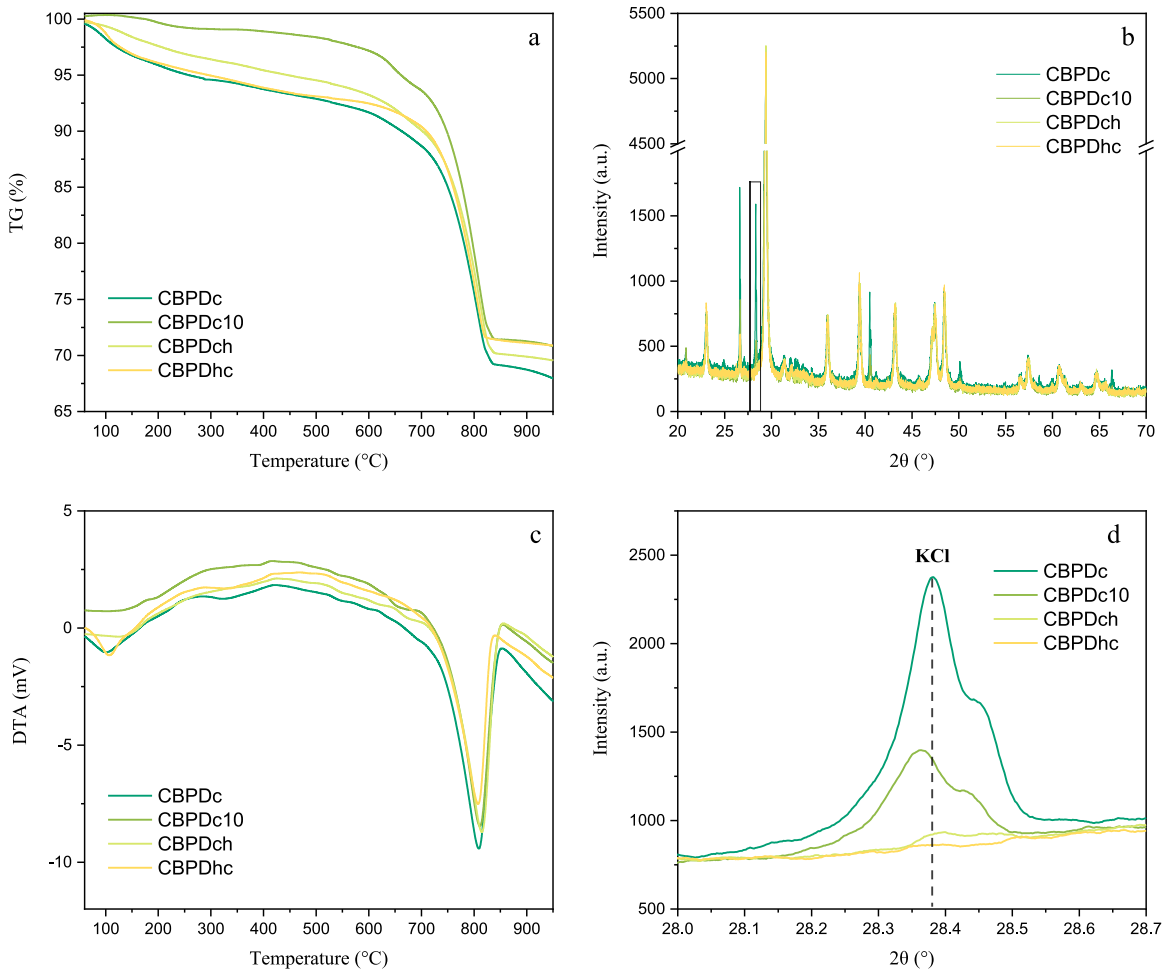

Fig. 7. Thermogravimetric analysis (a), XRD pattern (b), differential thermal analysis (c), XRD pattern in the potassium chloride range (d) of CBPDc, CBPDc10, CBPDch, CBPDhc.

Table 6
Content of carbon dioxide and potassium chloride, calculated respectively from thermogravimetric analysis and XRD calibration.

Configuration	CO_2 content (%)	CO_2 uptake (%)*	KCl content (%)
CBPDc	23.2 %	24.1 %	12.6 %
CBPDc10	26.4 %	24.7 %	5.7 %
CBPDch	23.9 %	22.2 %	0.7 %
CBPDhc	21.5 %	18.3 %	0.0 %

* Calculated according to Eq. 2, with the data from Supplementary Material Figure S2)

CO_2 uptake of CBPPDc10 with respect to CBPDc. Unfortunately, CBPDc10 still maintained a significant content of KCl (Fig. 7.d).

In contrast, the two configurations with a double step (hydration and carbonation) enabled the removal of nearly all the potassium chloride. In particular conducting the hydration step before the carbonation resulted more efficient in removing the salts. In fact, it was already observed that CO_2 injection during municipal solid waste incineration (MSWI) fly ash washing favoured the decomposition of hardly soluble minerals like, for example, Friedel's salt ($3CaO{\cdot}Al_2O_3{\cdot}CaCl_2{\cdot}10H_2O$) and hydrocalumite [44], both identified in hydrated CBPD (Fig. 3). CBPDch demonstrated a lower CO_2 uptake in comparison to CBPDc (see Table 6), attributable to the leaching of calcium carbonate during the final hydration step. Another key aspect that needs investigation is the lower carbonation degree of CBPDhc with respect to all the other configurations. The hydration step resulted in the formation of different hydration phases (see Figure S3 in Supplementary Material), i.e. C-S-H, gypsum, C-A-S-H (calcium aluminium silicate hydrates) and portlandite [39], while the Friedel's salt observed in CBPDhy was not identified, probably due to the higher dilution (L/S ratio at 10 instead of 3). However, the hydration of silicate phases, particularly larnite, was likely incomplete, as evidenced by the observations in CBPDhy (Fig. 3.b). After carbonation, the DTA shows a reduced peak of the hydrated phases, however, this peak of CBPDhc (at 100 – 200°C), is still significant in comparison with the other carbonated CBPD (Fig. 7.c). This finding indicates that the C-S-H present in CBPDhc were only partially consumed or decalcified, suggesting that the $CaCO_3$ formed in CBPDhc was mostly derived from free lime and portlandite, with minor contribution from C_2S. CBPDhc, with one hour of carbonation, attained the same carbonation degree that was already achieved after about 40 min of carbonation in the absence of a hydration pre-treatment [18]. Notably, the hydration pretreatment exerts a substantial influence on the kinetics of the reactions, consequently delaying the carbonation process. This behaviour may be attributed to the hydration and carbonation reaction dynamics of C_2S in a CO_2-rich environment. As demonstrated by Gong et al. (2025) [45], the hydration of C_2S is retarded in an environment with a high CO_2 content. Concurrently, the carbonation reaction of C_2S is faster than the hydration reaction. Consequently, C_2S appears to carbonate at a faster rate than its hydration products. In CBPDch, where aqueous carbonation was the initial step, C_2S was subjected to the concurrent mechanisms of hydration and carbonation, based on CO_2 concentration in the solution [46]. In the presence of CO_2, C_2S was found to be more reactive to carbonation than to hydration [47], and the outcome of $CaCO_3$ from this

phase was higher. Conversely, in CBPDhc, the mineralisation concerned the hydrated phases that, with a slower rate of carbonation, led to a lower carbonation degree.

Results in Table 6 emphasise a relevant aspect pertaining to the adopted process. Despite the mild operational parameters, the adopted aqueous mineralisation process is characterised by a relevant carbonation efficiency, irrespective of the considered configuration. Concurrently, a substantial decrease in KCl content is evident. This is of particular relevance in double-step configurations that permit the complete salt removal. In this regard, the use of direct aqueous carbonation is found to be essential. Firstly, in contrast to other carbonation processes that take place in dry environments, this process guarantees favourable conditions (already at ambient pressure and temperature) for the formation of carbonic acid in water and its reaction with the hydrated phases. Secondly, the integration of aqueous carbonation with the washing treatment is a straightforward process, facilitating the optimisation of the overall process.

3.2. Hydration heat and compressive strength

3.2.1. Effects of aqueous carbonation

CBPD hydration reactivity was investigated through isothermal calorimetry coupled with mortar compressive strength tests. The treated samples, CBPDhy and CBPDc, are obtained from the process described in Section 2.2.1, with a L/S equal to 3. The outcomes of the R^3 isothermal calorimetry experiment are presented in Fig. 8. These results are expressed in terms of specific heat rate and cumulative heat release for the as-received, hydrated and carbonated CBPD. From Fig. 8, it is evident that CBPDar has high initial heat release, due to the hydration of the free lime [4,12]. The smaller and comparable heat releases measured in CBPDhy and CBPDc, instead, can be attributed to the hydration of larnite, still detected after the aqueous carbonation. Fig. 8.b shows the specific cumulative heat of the three materials, which amounted to 180, 72 and 75 J/g of SCM for CBPDar, CBPDhy and CBPDc respectively. According to these results, the treated CBPD is to be considered a non-reactive material when referring to the reactivity thresholds of 98 [27] and 120 [48] J/g of SCM. This result is consistent with the composition of the materials. Indeed, as observed from TGA analysis and XRD calibration, CBPDhy contains about 26 % of $Ca(OH)_2$, 9 % of $CaCO_3$ and 11 % of KCl, while CBPDc is composed by about 53 % of $CaCO_3$ and 10.7 % of KCl, therefore only a minor part of the materials could show residual hydration reactivity. The incomplete removal of chlorides in the carbonated powder could be due to the presence of sulphates (because of anhydrite) that limit the efficiency of the washing step [44]. However, CBPDar is not expected to show better mechanical performance since the heat release is not associated with the production of C-S-H or similar hydraulic phases.

In order to investigate the effects of partial binder substitution with SCMs on the cement paste during the early hydration phases, an additional isothermal calorimetry test, namely cement replacement (see Section 2.2.3), was conducted. As illustrated in Fig. 9, the specific heat release, as well as the specific cumulative heat, were measured. Despite the complexity of SCMs' impact on the strength development of blended cement pastes, the reactivity of most SCMs during the initial few days is typically negligible [29]. Therefore, the hydration intensity in these early stages is predominantly influenced by factors such as the water-to-cement ratio (i.e. the dilution effect), the filler effect and the nucleation effect, which can also be imparted by inert fillers [49]. The effect of CBPDar addition to the cement is the most impactful concerning the specific heat rate. As previously mentioned, the high heat rate is associated with CaO hydration, a strongly exothermic reaction. CBPDhy-30 and CBPDc-30 exhibited a more analogous trend in comparison to the reference paste, despite the fact that the primary hydration peak was anticipated by approximately 1.5 h in both cases. The specific cumulative heat of the treated CBPD reached values similar to those of the reference, remaining below it, suggesting no reactivity from these materials.

The results of compressive strength tests at 28 days on mortars are shown in Fig. 10.a. It was evident that all the replaced mortars exhibited a significant loss of mechanical strength in comparison to the reference. Of particular note was the powder as received, which exhibited a high content of chlorides and free lime that exerted a deleterious effect on the development of strength [50]. As illustrated in Fig. 10.b, the strength development of the samples at 30 % replacement and the reference mortars was observed at 3, 7 and 28 days. The trend exhibited by CBPDhy and CBPDc was found to be comparable, with CBPDhy demonstrating marginally diminished strength in the initial stages, yet enhanced reactivity at prolonged curing times. The relative strength ($R_{SCM,relative}$) for CBPDhy and CBPDc at 30 % of replacement was averagely reduced by 31 % and 33 %, respectively, thereby confirming the neutral effect of treated CBPD previously observed by calorimetry. Analogous outcomes were attained for the substitution of CBPDc at 20 % and 10 %, yielding a $R_{SCM,relative}$ of −22 % and −13 %, respectively. The trend of compressive strength at different replacement rates of CBPDc is in line with previous observations on limestone [51], as expected given its high content of calcium carbonate. These findings suggest that carbonated cement bypass dust could act solely as a filler in cement, if finer, and furthermore, its substitution can only be achieved

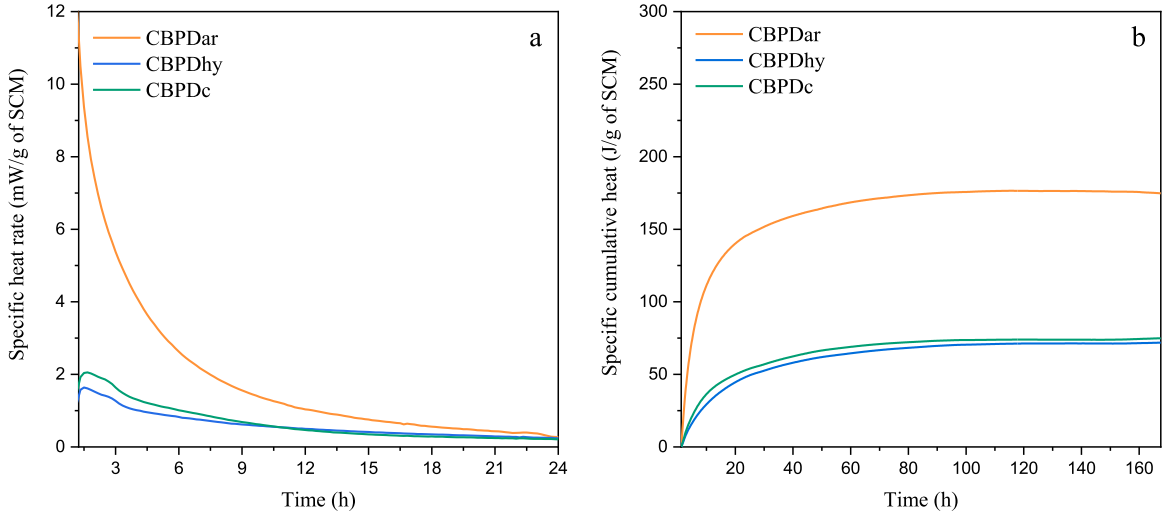

Fig. 8. Specific heat rate (a) and specific cumulative heat (b) by isothermal calorimetry of R^3-test pastes with CBPDar, CBPDhy and CBPDc.

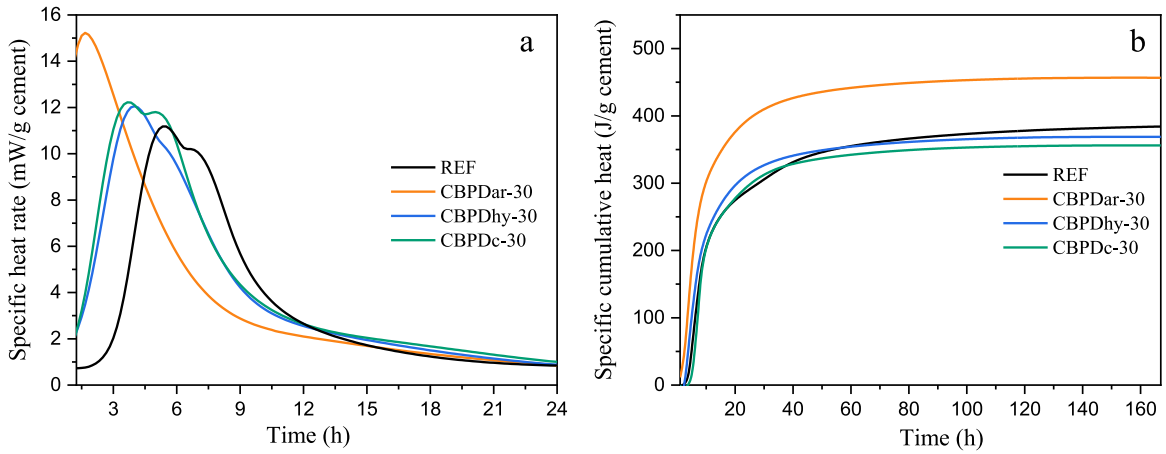

Fig. 9. Specific heat rate (a) and specific cumulative heat (b) by isothermal calorimetry of cement pastes with 30 % partial replacement of CBPDar, CBPDhy and CBPDc and of the reference cement paste (REF).

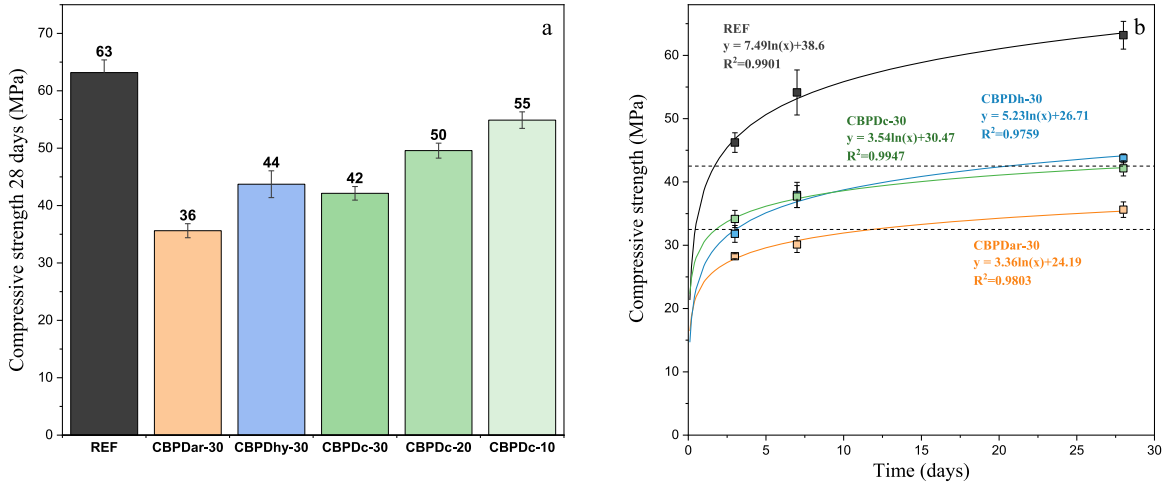

Fig. 10. Compressive strength of mortars cured at 28 days (a) compressive strength development of mortars cured for 3, 7 and 28 days (b).

at reduced replacement rates. Indeed, the residual content of KCl in CBPDc is estimated to be approximately 10.7 %. Given that the maximum chloride content permitted in cement is less than 0.1 % [52], the highest substitution percentage that can be proposed for CBPDc is 2.0 %.

3.2.2. *Effects of the optimised salt removal process*

The preliminary tests conducted previously were undertaken

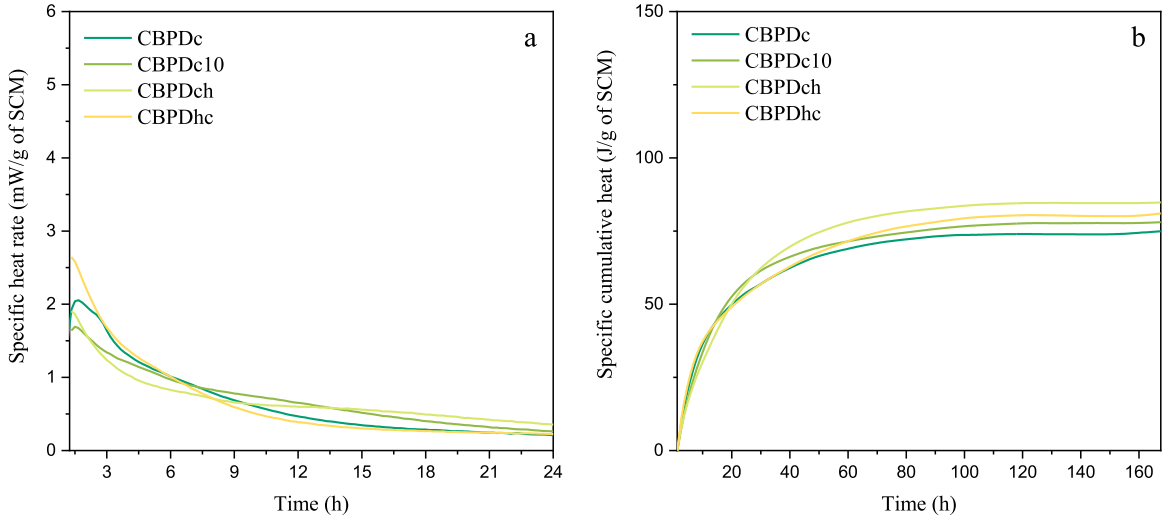

Fig. 11. Specific heat rate (a) and specific cumulative heat (b) by isothermal calorimetry of R^3-test pastes with CBPDc, CBPDc10, CBPDch, CBPDhc.

without consideration of the elevated level of potassium chloride content. Consequently, the subsequent investigation centred on the production of carbonated CBPD with reduced levels of KCl, leading to the development of the following three configurations: CBPDc10, CBPDch, CBPDhc. The isothermal calorimetry tests were then repeated with these new carbonated CBPD. The R^3-test results are exhibited in Fig. 11.a in which CBPDc was reported for the sake of comparison. As demonstrated in Fig. 11.a, CBPDhc exhibited a higher specific heat rate; however, CBPDch (Fig. 11.b) demonstrated a higher specific cumulative heat of 85 J/g of SCM, with CBPDc exhibiting the lower value, as anticipated given its higher content of non-reactive KCl. While all the new configurations did surpass the result of CBPDc, their specific heat was still below the threshold for reactive materials (98 J/g of SCM).

Fig. 12 exhibits the results from the isothermal calorimetry with cement partial replacement at 30 %. It is clear from Fig. 12.a that there is no significant difference in the specific heat rate of the three replaced samples. The main hydration peak is still anticipated in all the replaced samples, in line with previous studies on limestone substitution [53]. It is noteworthy that CBPDhc is the only material which reaches a maximum specific heat rate that is similar to that of cement (REF). Fig. 12.b shows that CBPDc10–30 and CBPDhc-30 exhibited a specific cumulative heat higher than cement, at 418 and 417 J/g of cement, respectively. CBPDch-30 exhibited a pattern similar to the other replaced samples, however it obtained a slightly lower specific cumulative heat, 410 J/g of cement. The findings are encouraging in terms of their implications, as they suggest that the treated CBPDs gained reactivity with respect to the previous tests (Fig. 9).

Following the calorimetry tests, mortars with 30 % of replacement of CBPDc10, CBPDch and CBPDhc were prepared and cured for 28 days. The results from Fig. 13.a show a decline in the mechanical properties of the mortars due to the incorporation of carbonated CBPD. In general, the mortars with partial substitution exhibited comparable ranges of strength development. However, CBPDhc-30 is the first sample to demonstrate a $R_{SCM,relative}$ that is notably above −35 % (Fig. 13.b), which has been regarded as the reactivity threshold when comparing mortars with a replacement rate of 30 % [27]. This outcome can be correlated with calorimetry tests, in which, the heat rate of CBPDhc was enhanced in comparison to the other samples, despite the cumulative heat release being comparable. In fact, CBPDhc showed the specific heat peak with highest intensity in R^3-test calorimetry (Fig. 11 a). Moreover, the same peak was even comparable in intensity with the plain cement reference sample in the isothermal calorimetry test conducted on cement paste samples (Fig. 12 a). This signal, related to the C-S-H precipitation [54], indicates the higher hydration rate occurring in CBPDhc sample. In fact, the increased strength development could be associated with the previous hydration step and the subsequent carbonation. Indeed, previous studies on carbonated recycled cement paste powder [55] highlighted beneficial effects on the compressive strength for increased content of $CaCO_3$ and silica gel, and CBPDhc was the material showing the higher residual hydrated phases (observed by TGA, Fig. 7. a).

3.2.3. Comparison with conventional SCMs

The results from reactivity tests are herein compared with studies from the literature [27,31]. Fig. 14 presents the correlation between 28-days relative strength and 7-day cumulative heat (H_{7d}) of conventional SCMs. The SCMs selected are specifically from the subgroup composed of slags (SL), pozzolans (PZ) and fly ashes (FA). The y-axis is associated with the 28 days relative compressive strength and the threshold of inert materials is usually associated with the average results from quartz (which shows a $R_{SCM,relative}$ = -35 %). CBPD results were incorporated into the graph to evaluate the material's classification relative to other conventional SCMs. Only CBPDhc was selected between the upgraded versions of the carbonated CBPD, on account of its superior relative strength. It is evident that the CBPDar does not align with the regression, probably because of the high salts content, exhibiting a distinct behaviour in relation to the reported SCM classes. Conversely, all the treated CBPDs exhibited a strong correlation with the linear regression, although occupying the lower end of the reactivity range. Despite the carbonated material maintaining a low reactivity range, it is notable that, as a consequence of the aqueous carbonation process, CBPD aligns with the behaviour of other SCMs, whilst the raw CBPD is evidently less reactive (particularly in light of the high content of salts).

3.3. Effect of calcite and chloride content

In this section, the study investigates the effects of the CBPD composition on the mechanical properties that were previously observed. The CBPD composition was obtained from XRD calibration for the KCl content and from thermogravimetric analysis for the CO_2 content (see Fig. 15). It is evident from Fig. 15.a that for higher amounts of KCl, the relative strength decreased. Nevertheless, potassium chloride doesn't have a detrimental effect on mechanical strength during the curing process. The damaging effects of potassium chloride have consistently been demonstrated to be a result of volume expansion during freeze-thaw cycles in concrete [56] and corrosion of reinforcing bars in reinforced concrete [57]. However, the decline observed in the compressive strength could be explained by a decrease in reactive compounds of CBPD which were substituted by KCl.

Fig. 15.b investigates the potential correlation between the content of CO_2 and the relative strength. Given the significant correlation between KCl content and relative strength, it becomes challenging to

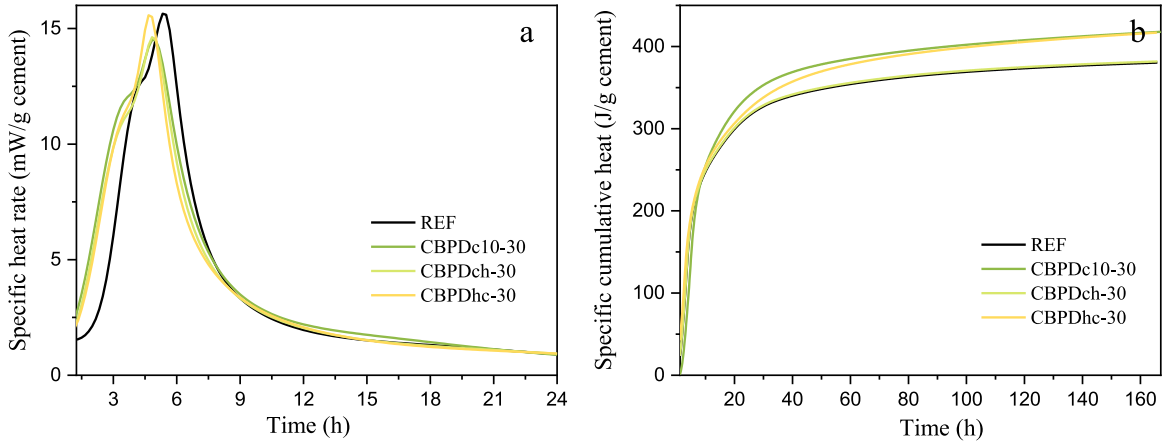

Fig. 12. Specific heat rate (a) and specific cumulative heat (b) by isothermal calorimetry of cement pastes with 30 % partial replacement of CBPDc10, CBPDch, CBPDhc, and of the reference cement paste (REF).

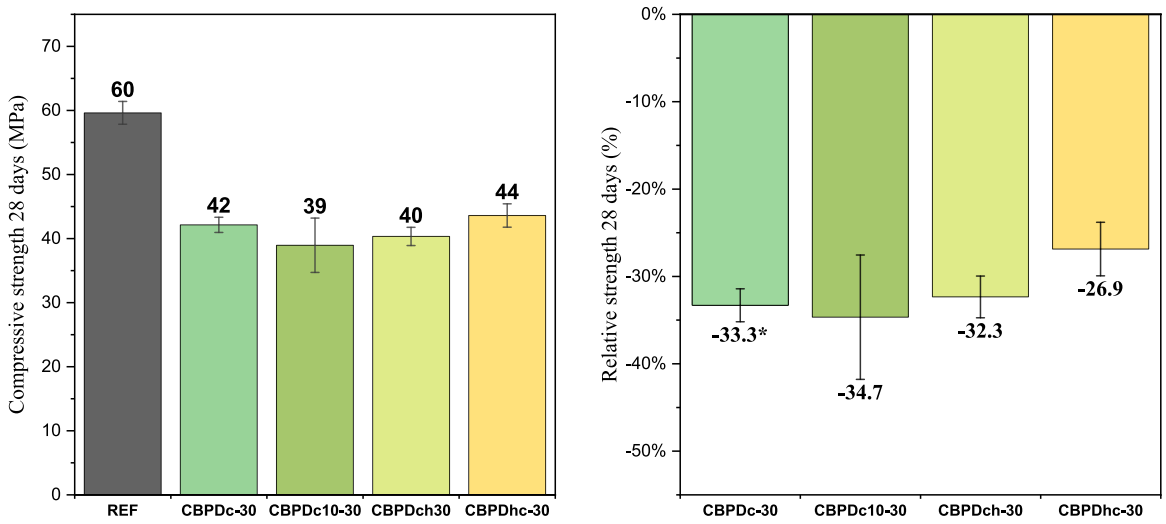

Fig. 13. Compressive strength at 28 days (a) and relative compressive strength (b) of mortars containing carbonated CBPD.*calculated with respect to its REF in Fig. 10.

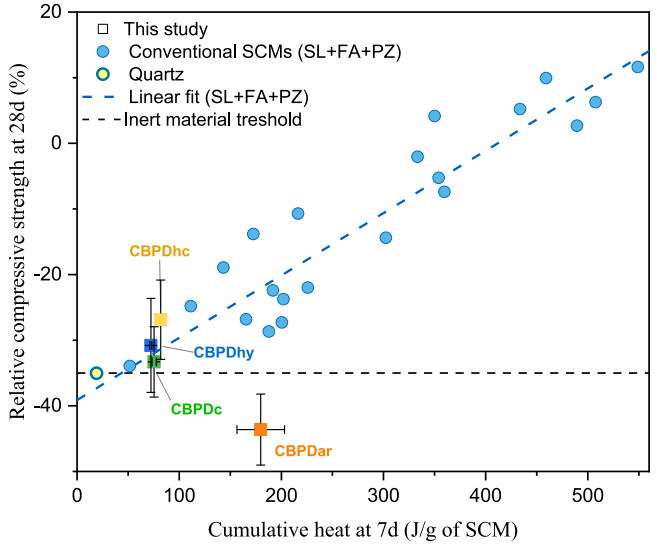

Fig. 14. Linear correlation of R^3 tests – cumulative heat to relative compressive strength at 28 days. Conventional SCMs (data from [27,31]) integrated with the results from this study.

determine whether $R_{SCM.relative}$ is more influenced by the content of CO_2 or KCl. In order to mitigate the impact of potassium chloride, the analysis was restricted to CBPDhc, CBPDch and CBPDc10, which exhibited lower and similar levels of KCl. As can be visualised in Fig. 15.b, a downward trend in relative strength is evident for higher carbonation degrees. This trend seems to confirm a correlation between residual reactivity of CBPD and reduced calcium carbonate formation, thereby validating the hypothesis concerning the presence of unreacted calcium silicate hydrates and larnite within the CBPDhc. It is important to note, however, that the error bands associated with the relative strength measurements are quite substantial, which complicates the interpretation of these results and hinders the ability to draw definitive conclusions on this matter.

It is imperative to emphasise that, in view of the minimum chloride content threshold permitted in cement blends (0.1 % [52]), the double-step treated powders, CBPDhc and CBPDch, represent the sole configurations that adhere to this limitation. Indeed, CBPDhc, which contains a residual KCl content of 0.56 % (see Table S2 of the Supplementary Material), can be substituted up to 37 % while adhering to the specified limitation. CBPDch demonstrates complete removal of KCl without constraints on the percentage of substitution related to chlorides content.

3.4. Environmental footprint of carbonated CBPD-based mortars

On the basis of an average CBPD production ranging from 2 % to 5 % of clinker production, an average CBPDhc CO_2 uptake of 18.3 %, and the emission of 0.83 ton of CO_2 to produce 1 ton of clinker [58], it is estimated that a CO_2 emission reduction of 0.4–1.1 % could be achieved. This outcome may appear negligible in absolute terms; however, it should be contextualised within the global scenario. In 2023, the worldwide production of clinker was estimated to be 3.8 billion metric tons [59], implying that 14–35 million tons of CO_2 per year could be sequestered by CBPD directly produced within the cement plant. However, the most significant effect would be noted in case of partial substitution of cement with carbonated CBPD, thanks to the avoided emissions. Fig. 16 shows a preliminary investigation into the environmental benefits of substituting cement with carbonated CBPD revealing a correlation between CO_2 emissions and the substitution percentage (Fig. 16.a) and strength class (Fig. 16.b) of diverse cement types (CEM I, CEM II, and CEM III). This analysis is further supported by the findings of this study. Derived from Environmental Product Declarations of European cement production and made available in the Supplementary Material (Table S1), the data set under consideration includes a segment of CEM II substituted with limestone, alongside CEM III, which was introduced to facilitate a comparative analysis of its performance as the sole cement type permitting a Cl^- content greater than 0.1 %. With regard to the data presented in the current study, the substitution percentage was specified as 10 %, 20 % and 30 %, whereas the CO_2 emissions were calculated from Eq. 5. In order to facilitate a comparison of cement emissions, the average value of cement emissions documented in 1990 (783 kg CO_2/t of cement) was selected as a reference. CBPD after carbonation exhibited a calcium carbonate content (as determined by TG analysis) ranging from 49 % to 60 %. Given this substantial percentage, it was hypothesised that its behaviour as a SCM would have been analogous to that of a limestone. In accordance with the cement types delineated in the European standard UNI EN 197–1 [52], the CBPDc-10 and CBPDc-20 samples could be classified as CEM II/A-L, wherein clinker is substituted with 6–20 % by mass of limestone. Conversely, CBPDc-30 could be classified as CEM II/B-L, with the substitution of 21–35 % by mass of limestone in place of clinker. Fig. 16.a

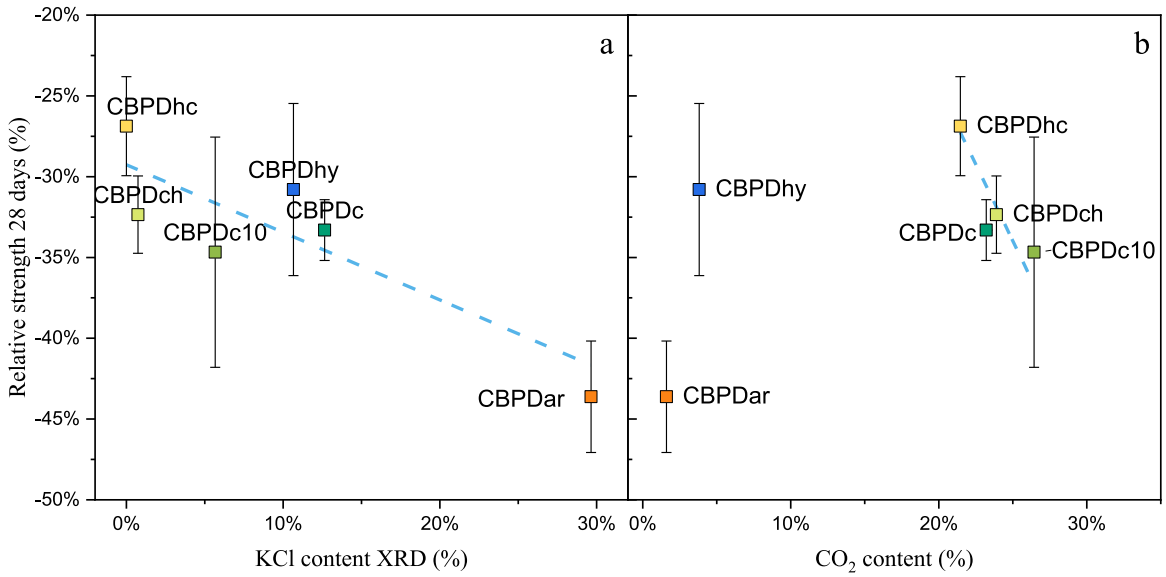

Fig. 15. Relation of relative compressive strength at 28 days with a) potassium chloride content and b) calcium dioxide content.

illustrates the linear correlation between the CO_2 emissions of cements and their clinker substitution ratio, which predictably shows that the higher the replacement rate, the lower the CO_2 emissions. In point of fact, materials employed in the role of SCMs generally demonstrate a negligible carbon footprint in comparison with that of cement. However, when the Cl^- content of the cement is taken into consideration (see Table 7), it is evident that only CBPDhc-30 and CBPDch-30 adheres to the prescribed limits on chlorides content (0.1 % [52]).

As Fig. 15.b illustrates, there is no direct correlation between low emissions and low compressive strength, particularly when considering the average values of CEM II 52.5 and CEM II 42.5. However, the data from this study does reveal a clear trend, which can be attributed to the low reactivity of the material added (i.e. carbonated CBPD). CBPDc-10, while slightly above the 52.5 strength class threshold, could be more accurately positioned within the 42.5 strength class. Notably, CBPDc-10 exhibits comparable CO_2 emissions to those of CEM I and CEM II 42.5. CBPDc-20 and CBPDhc-30 could also be ranked within the 42.5 strength class, but their CO_2 emissions are considerably lower than those of CEM I, particularly CBPDc-30 and CBPDch-30, which are within the average emissions interval of a CEM III 42.5, despite not meeting the classification criteria for CEM III. CBPDhc-30 instead, complies with both average emission and strength intervals of CEM II 42.5. Therefore, the treated powder may be adopted to produce this class of cement. In addition, based on the findings, it can be reasonably assumed that lower percentage of substitution may be useful to produce standardised cements of higher strength class. This confirms that the double step process is the right compromise to efficiently removing salt content, capturing CO_2 and promoting the reuse of the treated powder in cement blends while complying with strength and environmental requirements.

As previously mentioned, CBPDhc-30 and CBPDch-30 were the sole candidates that could be selected as an SCM with a high substitution rate thanks to its lower chlorides content. However, in view of the need for new carbon capture strategies to be identified by the cement industry, and the need for new supplementary cementitious materials to be promoted by the same industry, carbonated CBPD was identified as a viable option in relation to its environmental impact and performance. The dual process of hydration and carbonation, with the parameters used, can be regarded as an optimised compromise that combines the performance requirements of durability (chloride content), mechanical resistance and environmental impact. Furthermore, given the parallel trend exhibited by "conventional" carbonated CBPD, it is reasonable to hypothesise that resistance levels even higher than CBPDc10 will be attained. In summary, the dual-step process is a viable method of meeting durability requirements. Through the strategic variation of replacement percentages, it is possible to achieve a more robust or sustainable configuration, while preserving the resistance levels exhibited by conventional cements, as illustrated in Fig. 16.

4. Conclusions

This study presented a preliminary evaluation of the reactivity of cement bypass dust after mineral carbonation to test potential applications as SCM. During the carbonation process, the reactive phases such as free lime, portlandite and mayenite were consumed to form calcium carbonate and the particle size distribution shifted towards bigger fractions and became more homogeneous. The CO_2 content of the CBPD after mineralisation was 23.2 %. However, the content of potassium chloride was still high and new configurations of the carbonation process were investigated.

- The preliminary study on the KCl content after CBPD hydration at different liquid-to-solid ratio, showed that a L/S ratio of 20 was not enough to completely remove the KCl, however already the L/S ratio of 10 allowed to reduce it substantially. In order to avoid excessive water usage, an aqueous carbonation with L/S ratio 10, and two double step processes of hydration (L/S=10) and carbonation (L/S=3), alternated, were performed. The CO_2 content of the final materials ranged from 21.5 % and 26.4 %, and the sample CBPDhc was characterised by the complete removal of KCl. Furthermore, CBPDc produced via the one-step process with a L/S of 3 can be substituted to cement up to 2.0 % to meet the chloride content requirements. In contrast, the powder produced via the double step process can be substituted up to 37 % (CBPDhc) or without any limitation (CBPDch) while adhering to the specified restrictions.
- The reactivity tests comparing the CBPD as received, hydrated and carbonated, showed that despite CBPDar obtained a very high heat release, both with R^3 and cement replacement calorimetry analyses, this was not correlated with the compressive strength development of the mortars, which was the lowest registered. CBPDhy and CBPDc, instead showed a good correlation between the heat release and the strength development but obtained mild results. No significant reactivity was observed for carbonated CBPD. The samples with different partial substitution showed a linear trend with compressive strength at 28 days.

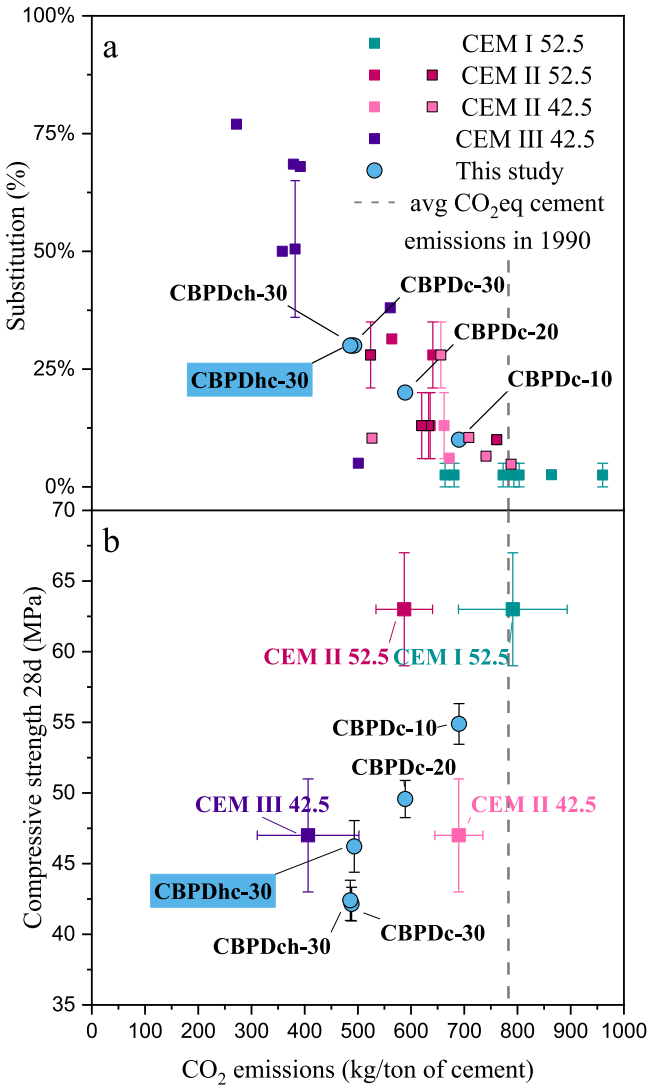

Fig. 16. CO_2eq emissions of different cement types based on their replacement rate (a), and their compressive strength (b), integrated with the results of this study.

Table 7
Chlorides content in the binder, derived from XRD analysis.

	Cl^- content of CEM with CBPD (%)
CBPDc-30	1.52 %
CBPDc-20	1.01 %
CBPDc-10	0.51 %
CBPDhc-30	0.00 %
CBPDch-30	0.08 %

- The samples with reduced chlorides content, showed similar reactivity when analysed with calorimetry. However, CBPDhc stood out as the material with higher heat rate and it also provided the better mechanical performances with a relative strength of −26.9 %. CBPDhc better performances were associated with both lower content of chlorides and lower carbonation degree, which seemed to have affected the material's reactivity. The lower carbonation degree is attributed to the first hydration step which probably made part of the calcium unavailable during the successive carbonation step.
- The aqueous carbonation treatment, which stabilised the initial content of free lime and removed partly or completely KCl, finally made possible the reuse of CBPD as SCM. A comparative analysis of CO_2 emissions, substitution percentage and strength class, based on the data from different types of standard cement, was conducted on the data of this study in order to frame CBPD-based cements within the current commercial classifications. CBPDhc has been identified as a potential product for achieving comparable strength and environmental performance to that of CEM III 42.5 when substituted at a rate of 30 %.

However, the limited amount of CBPD produced could be a drawback when considering the economic feasibility and actual environmental impact of an industrially integrated mineralisation process. Consequently, further research should concentrate on a comprehensive life cycle assessment, incorporating of potassium chloride possible reuses (i.e. as fertiliser). Nevertheless, the overarching goal should be to achieve a zero-waste production and to determine the potential for sequestering CO_2 in various alkali wastes or by-products.

CRediT authorship contribution statement

Giuseppe Ferrara: Writing – review & editing, Supervision, Conceptualization. **Davide Garufi:** Writing – review & editing, Visualization, Supervision, Project administration. **Pedro Humbert:** Writing – review & editing, Visualization, Validation, Supervision, Conceptualization. **Francesca Bonfante:** Writing – original draft, Methodology, Investigation, Formal analysis, Data curation, Conceptualization. **Paola Palmero:** Writing – review & editing, Validation, Supervision, Project administration, Investigation, Conceptualization. **Jean-Marc Tulliani:** Writing – review & editing, Visualization, Validation, Supervision, Conceptualization.

Declaration of Competing Interest

The authors declare that they have no known competing financial interests or personal relationships that could have appeared to influence the work reported in this paper.

Acknowledgements

The research described in this paper was financially supported by the European Union's for the PON "Ricerca e Innovazione" 2014–2020 Azione IV.4 - REACT EU projects (DM 1061) and by CRH Innovation Centre for Sustainable Construction Europe. The authors gratefully acknowledge the Safety of Infrastructures and Constructions (SISCON) laboratory for providing the instrumentation for thermal and granulometry analysis.

Appendix A. Supporting information

Supplementary data associated with this article can be found in the online version at doi:10.1016/j.conbuildmat.2025.145004.

Data availability

Data will be made available on request.

References

[1] F. Zunino, F. Martirena, K. Scrivener, Limestone calcined clay cements (LC3), Mater. J. 118 (2021) 49–60, https://doi.org/10.14359/51730422.
[2] CEMBUREAU's Net Zero Roadmap, Brussels, 2024. ⟨https://cembureau.eu/library/reports/cembureau-s-net-zero-roadmap/⟩ (accessed July 30, 2025).
[3] A.M.K. Abiad, K. Pilakoutas, M. Guadagnini, H. Kinoshita, The influence of cement bypass dust composition on the properties of slag-based mortars, Constr. Build. Mater. 444 (2024) 137829, https://doi.org/10.1016/J.CONBUILDMAT.2024.137829.
[4] K. Wojtacha-Rychter, M. Król, M. Gołaszewska, J. Całus-Moszko, M. Magdziarczyk, A. Smoliński, Dust from chlorine bypass installation as cementitious materials

replacement in concrete making, J. Build. Eng. 51 (2022) 104309, https://doi.org/10.1016/J.JOBE.2022.104309.
[5] M. Heikal, I. Aiad, I.M. Helmy, Portland cement clinker, granulated slag and by-pass cement dust composites, Cem. Concr. Res 32 (2002) 1805–1812, https://doi.org/10.1016/S0008-8846(02)00867-0.
[6] H.Y. Ghorab, A. Mounir, N. Ghabrial, M. Rizk, S. Badawi, M. Khafaga, Resuse of Cement Kiln Bypass Dust in the Manufacture of Ordinary Portland Cement, Polym. Plast. Technol. Eng. 43 (2004) 1723–1734, https://doi.org/10.1081/PPT-200040077.
[7] K. Borek, P. Czapik, R. Dachowski, Cement Bypass Dust as an Ecological Binder Substitute in Autoclaved Silica-Lime Products, (2022). https://doi.org/10.3390/ma16010316.
[8] A.S. Al-Harthy, R. Taha, J. Abu-Ashour, K. Al-Jabri, S. Al-Oraimi, Effect of water quality on the strength of flowable fill mixtures, Cem. Concr. Compos 27 (2005) 33–39, https://doi.org/10.1016/J.CEMCONCOMP.2004.01.005.
[9] F. Bonfante, G. Ferrara, P. Humbert, J.M. Tulliani, P. Palmero, CO2 mineralization process of industrial by-products for the production of sustainable mortars, Nov 9th-10th, fib. in: 3rd Fib Symposium on Concrete and Concrete Structures, The International Federation for Structural Concrete, 2023, pp. 355–362. Nov 9th-10th, fib.
[10] T. Hanein, Y. Hayashi, C. Utton, M. Nyberg, J.C. Martinez, N.I. Quintero-Mora, H. Kinoshita, Pyro processing cement kiln bypass dust: Enhancing clinker phase formation, Constr. Build. Mater. 259 (2020) 120420, https://doi.org/10.1016/J.CONBUILDMAT.2020.120420.
[11] W.S. Adaska, D.H. Taubert, Beneficial uses of cement kiln dust, IEEE Cem. Ind. Tech. Conf. (Pap.) (2008) 210–228, https://doi.org/10.1109/CITCON.2008.24.
[12] P. Czapik, J. Zapała-Sławeta, Z. Owsiak, P. Stępień, Hydration of cement by-pass dust, Constr. Build. Mater. 231 (2020) 117139, https://doi.org/10.1016/J.CONBUILDMAT.2019.117139.
[13] R. Taha, A. Al-Rawas, A. Al-Harthy, H. Al-Siyabi, Use of cement by-pass dust in soil stabilization, Eng. J. Univ. Qatar 14 (2001) 61–76. ⟨https://squ.elsevierpure.com/en/publications/use-of-cement-by-pass-dust-in-soil-stabilization⟩ (accessed October 16, 2023).
[14] R. Taha, A. Al-Rawas, A. Al-Harthy, A. Qatan, Use of Cement Bypass Dust as Filler in Asphalt Concrete Mixtures, J. Mater. Civ. Eng. 14 (2002) 338–343, https://doi.org/10.1061/(ASCE)0899-1561(2002)14:4(338).
[15] G. Sturm, B. Galichet, The ReduDust Project – an innovativesolution for treatment of bypass dust, Cem. Int. 10 (2012) 60–65.
[16] E.M. Sipple, J. Mullner, A green building in a grey cement plant – Transforming bypass dust into industrial salt with the ReduDust Process, Rohoznik (SVK), 2016. ⟨https://www.atec-ltd.com/images/Redudust_ZKG_11.pdf⟩ (accessed November 27, 2023).
[17] C.R. Yörük, M. Uibu, M.C. Usta, T. Kaljuvee, A. Trikkel, CO2 mineralization by burnt oil shale and cement bypass dust: effect of operating temperature and pre-treatment, J. Therm. Anal. Calor. 142 (2020) 991–999, https://doi.org/10.1007/S10973-020-09349-9/FIGURES/8.
[18] F. Bonfante, P. Humbert, J.M. Tulliani, P. Palmero, G. Ferrara, CO2 uptake of cement by-pass dust via direct aqueous carbonation: an experimental design for time and temperature optimisation, Mater. Struct. Mater. Et. Constr. 57 (2024) 1–18, https://doi.org/10.1617/S11527-024-02457-0/TABLES/3.
[19] P.K. Araizi, C.D. Hills, A. Maries, P.J. Gunning, D.S. Wray, Enhancement of accelerated carbonation of alkaline waste residues by ultrasound, Waste Manag. 50 (2016) 121–129, https://doi.org/10.1016/J.WASMAN.2016.01.006.
[20] J. Wang, P. Zeng, Z. Liu, Y. Li, Manufacture of potassium chloride from cement kiln bypass dust: An industrial implementation case for transforming waste into valuable resources, Heliyon 9 (2023) e21806, https://doi.org/10.1016/J.HELIYON.2023.E21806.
[21] M. Daous, Recovery of potassium salts from kiln dust of local cement plants. in: The 6th Saudi Engineering Conference, KFUPM, Dhahran, Saudi Arabia, 2002, pp. 473–485.
[22] G. Ferrara, A. Belli, A. Keulen, J.-M. Tulliani, P. Palmero, Testing procedures for CO2 uptake assessment of accelerated carbonation products: Experimental application on basic oxygen furnace steel slag samples, Constr. Build. Mater. 406 (2023) 133384, https://doi.org/10.1016/J.CONBUILDMAT.2023.133384.
[23] P.S. Humbert, J.P. Castro-Gomes, H. Savastano, Clinker-free CO2 cured steel slag based binder: Optimal conditions and potential applications, Constr. Build. Mater. 210 (2019) 413–421, https://doi.org/10.1016/J.CONBUILDMAT.2019.03.169.
[24] G. Liu, K. Schollbach, S. van der Laan, P. Tang, M.V.A. Florea, H.J.H. Brouwers, Recycling and utilization of high volume converter steel slag into CO2 activated mortars – The role of slag particle size, Resour. Conserv Recycl 160 (2020) 104883, https://doi.org/10.1016/J.RESCONREC.2020.104883.
[25] G. Ferrara, P. Humbert, D. Garufi, P. Palmero, Evolution of CO2 Uptake Degree of Ordinary Portland Cement During Accelerated Aqueous Mineralisation, Ceramics 7 (4) (2024) 1711–1726, https://doi.org/10.3390/ceramics7040109.
[26] 267-TRM: Tests for reactivity of supplementary cementitious materials, (n.d.). ⟨https://www.rilem.net/groupe/267-trm-tests-for-reactivity-of-supplementary-cementitious-materials-339⟩ (accessed November 22, 2024).
[27] D. Londono-Zuluaga, A. Gholizadeh-Vayghan, F. Winnefeld, F. Avet, M. Ben Haha, S.A. Bernal, Ö. Cizer, M. Cyr, S. Dolenec, P. Durdzinski, J. Haufe, D. Hooton, S. Kamali-Bernard, X. Li, A.T.M. Marsh, M. Marroccoli, M. Mrak, Y. Muy, C. Patapy, M. Pedersen, S. Sabio, S. Schulze, R. Snellings, A. Telesca, A. Vollpracht, G. Ye, S. Zhang, K.L. Scrivener, Report of RILEM TC 267-TRM phase 3: validation of the R3 reactivity test across a wide range of materials, Mater. Struct. /Mater. Et. Constr. 55 (2022) 1–16, https://doi.org/10.1617/S11527-022-01947-3/FIGURES/10.
[28] F. Avet, X. Li, M. Ben Haha, S.A. Bernal, S. Bishnoi, Ö. Cizer, M. Cyr, S. Dolenec, P. Durdzinski, J. Haufe, D. Hooton, M.C.G. Juenger, S. Kamali-Bernard, D. Londono-Zuluaga, A.T.M. Marsh, M. Marroccoli, M. Mrak, A. Parashar, C. Patapy, M. Pedersen, J.L. Provis, S. Sabio, S. Schulze, R. Snellings, A. Telesca, M. Thomas, F. Vargas, A. Vollpracht, B. Walkley, F. Winnefeld, G. Ye, S. Zhang, K. Scrivener, Report of RILEM TC 267-TRM phase 2: optimization and testing of the robustness of the R3 reactivity tests for supplementary cementitious materials, Mater. Struct. Mater. Et. Constr. 55 (2022) 1–14, https://doi.org/10.1617/S11527-022-01928-6/TABLES/6.
[29] B. Lothenbach, K. Scrivener, R.D. Hooton, Supplementary cementitious materials, Cem. Concr. Res 41 (2011) 1244–1256, https://doi.org/10.1016/J.CEMCONRES.2010.12.001.
[30] ASTM C1897-20 - Standard Test Methods for Measuring the Reactivity of Supplementary Cementitious Materials by Isothermal Calorimetry and Bound Water Measurements - European Standards, (2020). ⟨https://www.en-standard.eu/astm-c1897-20-standard-test-methods-for-measuring-the-reactivity-of-supplementary-cementitious-materials-by-isothermal-calorimetry-and-bound-water-measurements/⟩ (accessed April 16, 2023).
[31] X. Li, R. Snellings, M. Antoni, N.M. Alderete, M. Ben Haha, S. Bishnoi, Ö. Cizer, M. Cyr, K. De Weerdt, Y. Dhandapani, J. Duchesne, J. Haufe, D. Hooton, M. Juenger, S. Kamali-Bernard, S. Kramar, M. Marroccoli, A.M. Joseph, A. Parashar, C. Patapy, J.L. Provis, S. Sabio, M. Santhanam, L. Steger, T. Sui, A. Telesca, A. Vollpracht, F. Vargas, B. Walkley, F. Winnefeld, G. Ye, M. Zajac, S. Zhang, K.L. Scrivener, Reactivity tests for supplementary cementitious materials: RILEM TC 267-TRM phase 1, Mater. Struct. /Mater. Et. Constr. 51 (2018) 1–14, https://doi.org/10.1617/S11527-018-1269-X/TABLES/5.
[32] BS EN, 196-1, Methods of testing cement: Determination of strength, British Standards Institution, 2016. ⟨https://www.en-standard.eu/bs-en-196-1-2016-methods-of-testing-cement-determination-of-strength/⟩ (accessed March 27, 2024).
[33] D. Barnat-Hunek, J. Góra, Z. Suchorab, G. Łagód, Cement Kiln Dust, Waste and Supplementary Cementitious Materials in Concrete: Characterisation, Prop. Appl. (2018) 149–180, https://doi.org/10.1016/B978-0-08-102156-9.00005-5.
[34] D.N. Huntzinger, J.S. Gierke, S.K. Kawatra, T.C. Eisele, L.L. Sutter, Carbon dioxide sequestration in cement kiln dust through mineral carbonation, Environ. Sci. Technol. 43 (6) (2009) 1986–1992, https://doi.org/10.1021/es802910z.
[35] A.K. Suryavanshi, R. Narayan Swamy, Stability of Friedel's salt in carbonated concrete structural elements, Cem. Concr. Res. 26 (1996) 729–741, https://doi.org/10.1016/S0008-8846(96)85010-1.
[36] S. Goñi, A. Guerrero, Accelerated carbonation of Friedel's salt in calcium aluminate cement paste, Cem. Concr. Res. 33 (2003) 21–26, https://doi.org/10.1016/S0008-8846(02)00910-9.
[37] N. Zhang, G. Deng, W. Liao, H. Ma, C. Hu, Aqueous carbonation of steel slags: a comparative study on mechanisms, Cem. Concr. Compos 155 (2025) 105838, https://doi.org/10.1016/J.CEMCONCOMP.2024.105838.
[38] M. Broström, S. Enestam, R. Backman, K. Mäkelä, Condensation in the KCl–NaCl system, Fuel Process. Technol. 105 (2013) 142–148, https://doi.org/10.1016/J.FUPROC.2011.08.006.
[39] B. Lothenbach, P. Durdzinski, K. De Weerdt, Thermogravimetric analysis. in: A Practical Guide to Microstructural Analysis of Cementitious Materials, CRC Press, 2018, pp. 196–231, https://doi.org/10.1201/B19074-5.
[40] J. Csizmadia, G. Balázs, F.D. Tamás, Chloride ion binding capacity of aluminoferrites, Cem. Concr. Res. 31 (2001) 577–588, https://doi.org/10.1016/S0008-8846(01)00458-6.
[41] T.M. Rossi, J.C. Campos, M.M.V.M. Souza, Synthesis and characterization of hydrocalumite: influence of aging conditions on the structure, textural properties, thermal stability, and basicity, Clays Clay Min. 68 (2020) 273–286, https://doi.org/10.1007/s42860-019-00049-6.
[42] Ç.M. Oral, B. Ercan, Influence of pH on morphology, size and polymorph of room temperature synthesized calcium carbonate particles, Powder Technol. 339 (2018) 781–788, https://doi.org/10.1016/J.POWTEC.2018.08.066.
[43] Y. Jiang, Z. Ma, Y. Gao, P. Shen, C.S. Poon, A review on the impact of water in accelerated carbonation: implications for producing sustainable construction materials, Cem. Concr. Compos 157 (2025) 105902, https://doi.org/10.1016/J.CEMCONCOMP.2024.105902.
[44] Y. Wei, X. Du, S. Liu, Y. Wen, Q. Liao, G. Jiao, S. Tang, Promotion of chloride removal from MSWI fly ash by an accelerated wet-carbonation process to enhance ash recycling in cement manufacture, J. Environ. Chem. Eng. 12 (3) (2024) 112591.
[45] P. Gong, K. Mei, L. Zhang, Q. Xue, X. Wang, T. Wei, X. Cheng, Hydration and carbonation reaction dynamics in CO2-rich environment for tricalcium silicate (C3S) and dicalcium silicate (C2S), Powder Technol. 452 (2025) 120535. ⟨https://www.sciencedirect.com/science/article/pii/S0032591024011793⟩.
[46] Z. Chen, Z. Cang, F. Yang, J. Zhang, L. Zhang, Carbonation of steelmaking slag presents an opportunity for carbon neutral: a review, J. CO2 Util. 54 (2021) 101738, https://doi.org/10.1016/J.JCOU.2021.101738.
[47] R.W.M. Jensen, J. Skibsted, Aqueous carbonation of calcium silicates with different Ca/Si ratios studied by solid-state NMR spectroscopy, Magn. Reson. Chem. 63 (7) (2025) 476–494, https://doi.org/10.1002/mrc.5528.
[48] P. Suraneni, A. Hajibabaee, S. Ramanathan, Y. Wang, J. Weiss, New insights from reactivity testing of supplementary cementitious materials, Cem. Concr. Compos 103 (2019) 331–338, https://doi.org/10.1016/J.CEMCONCOMP.2019.05.017.
[49] P. Lawrence, M. Cyr, E. Ringot, Mineral admixtures in mortars: Effect of inert materials on short-term hydration, Cem. Concr. Res. 33 (2003) 1939–1947, https://doi.org/10.1016/S0008-8846(03)00183-2.
[50] K. Wojtacha-Rychter, M. Król, M. Gołaszewska, J. Całus-Moszko, M. Magdziarczyk, A. Smoliński, Dust from chlorine bypass installation as cementitious materials

replacement in concrete making, J. Build. Eng. 51 (2022) 104309, https://doi.org/10.1016/J.JOBE.2022.104309.
[51] S. Ramanathan, M. Croly, P. Suraneni, Comparison of the effects that supplementary cementitious materials replacement levels have on cementitious paste properties, Cem. Concr. Compos 112 (2020) 103678, https://doi.org/10.1016/J.CEMCONCOMP.2020.103678.
[52] BS EN 197-1:2011 Cement Composition, specifications and conformity criteria for common cements - European Standards, n.d. ⟨https://www.en-standard.eu/bs-en-197-1-2011-cement-composition-specifications-and-conformity-criteria-for-common-cements/⟩ (accessed June 23, 2022).
[53] D.P. Bentz, C.F. Ferraris, S.Z. Jones, D. Lootens, F. Zunino, Limestone and silica powder replacements for cement: Early-age performance, Cem. Concr. Compos 78 (2017) 43–56, https://doi.org/10.1016/J.CEMCONCOMP.2017.01.001.
[54] H.C. Pedrosa, O.M. Reales, V.D. Reis, M. das Dores Paiva, E.M.R. Fairbairn, Hydration of Portland cement accelerated by CSH seeds at different temperatures, Cem. Concr. Res. 129 (2020) 105978, https://doi.org/10.1016/j.cemconres.2020.105978.
[55] Y. Mao, X. Hu, U.J. Alengaram, W. Chen, C. Shi, Use of carbonated recycled cement paste powder as a new supplementary cementitious material: a critical review, Cem. Concr. Compos 154 (2024) 105783, https://doi.org/10.1016/J.CEMCONCOMP.2024.105783.
[56] A. Antolik, D. Jóźwiak-Niedźwiedzka, ASR induced by chloride- and formate-based deicers in concrete with non-reactive aggregates, Constr. Build. Mater. 400 (2023) 132811, https://doi.org/10.1016/J.CONBUILDMAT.2023.132811.
[57] C.M. Hansson, T. Frølund, J.B. Markussen, The effect of chloride cation type on the corposion of steel in concrete by chloride salts, Cem. Concr. Res. 15 (1985) 65–73, https://doi.org/10.1016/0008-8846(85)90009-2.
[58] Technology Roadmap - Low-Carbon Transition in the Cement Industry – Analysis - IEA, (n.d.). ⟨https://www.iea.org/reports/technology-roadmap-low-carbon-transition-in-the-cement-industry⟩ (accessed January 15, 2025).
[59] Clinker capacity worldwide by country 2023 | Statista, (n.d.). ⟨https://www.statista.com/statistics/219347/clinker-capacity-worldwide/#statisticContainer⟩ (accessed July 30, 2025).